Rancourt, Denis G. ; Fortin, Danielle ; Pichler, Thomas ; Thibault, Pierre-Jean ; Lamarche, Gilles ; Morris, Richard V. ; Mercier, Patrick H.J.

Mineralogy of a natural As-rich hydrous ferric oxide coprecipitate formed by mixing of hydrothermal fluid and seawater: Implications regarding surface complexation and color banding in ferrihydrite deposits

Journal Article	as:	peer-reviewed accepted version (Postprint)
DOI of this document*(secondary publication):		https://doi.org/10.26092/elib/3270
Publication date of this document:		02/09/2024

* for better findability or for reliable citation

Recommended Citation (primary publication/Version of Record) incl. DOI:

Rancourt, Denis G., Fortin, Danielle, Pichler, Thomas, Thibaul, Pierre-Jean, Lamarche, Gilles, Morris, Richard V. and Mercier, Patrick H.J.. "Mineralogy of a natural As-rich hydrous ferric oxide coprecipitate formed by mixing of hydrothermal fluid and seawater: Implications regarding surface complexation and color banding in ferrihydrite deposits" American Mineralogist, vol. 86, no. 7-8, 2001, pp. 834-851. https://doi.org/10.2138/am-2001-0707

Mineralogy of a natural As-rich hydrous ferric oxide coprecipitate formed by mixing of hydrothermal fluid and seawater: Implications regarding surface complexation and color banding in ferrihydrite deposits

DENIS G. RANCOURT,[1,*] DANIELLE FORTIN,[2] THOMAS PICHLER,[2,†] PIERRE-JEAN THIBAULT,[1,2] GILLES LAMARCHE,[1] RICHARD V. MORRIS,[3] AND PATRICK H.J. MERCIER[1]

[1]Department of Physics, University of Ottawa, Ottawa, Ontario K1N 6N5, Canada
[2]Department of Earth Sciences, University of Ottawa, Ottawa, Ontario K1N 6N5, Canada
[3]SN3, NASA—Johnson Space Center, Houston, Texas 77058, U.S.A.

ABSTRACT

We characterized the most As-rich natural hydrous ferric oxide (HFO) material ever reported using powder X-ray diffraction (pXRD), transmission electron microscopy (TEM), X-ray fluorescence spectroscopy (XRF), light element analysis using gas chromatography (GC), visible-infrared (vis-IR) diffuse reflectivity, ^{57}Fe Mössbauer spectroscopy, and superconducting quantum interference device (SQUID) magnetometry. We find that the natural As-HFO material is very similar to synthetic coprecipitated As-HFO materials, but is significantly different from all known natural and synthetic As-free HFO materials and ferrihydrite samples. The pXRD patterns show systematic differences with patterns for 2-line ferrihydrite, that are interpreted as evidence for significant populations of oxygen-coordinated Fe-As pairs. Observations by TEM, combined with energy dispersive spectroscopy (EDS) microanalysis, show agglomerations of nanophase primary particles and no evidence for other Fe- or As-bearing phases. Mössbauer spectroscopy shows octahedrally coordinated Fe^{3+}, with a large fraction (~20%) of the octahedral Fe environments that are significantly distorted by the presence of As, compared to the Fe local environments in As-free ferrihydrite and HFO samples. The loss on ignition (LOI) is quantitatively consistent with OH + H_2O, measured by GC, which, in turn, is consistent with ~1 nm diameter primary particles having all their surface cations (Fe^{3+}, As^{5+}, Si^{4+}, C^{4+}) coordinated on the free surface side by OH^- and OH_2. The banding into adjacent yellowish and reddish layers that occurs in the As-HFO deposits was studied by performing mineralogical analyses of the separated adjacent layers of two couplets of yellowish and reddish material. The yellowish samples were found not to contain secondary crystalline phases (as did the reddish samples, in small amounts) and to be relatively As-rich, C- and Si-poor. The observed anticorrelations between As and Si and between As and inorganic C suggest that natural HFOs, which usually contain significant molar amounts of Si, may not be as efficient at surface complexing As (and P) as their Si and C-free synthetic counterparts, unless formed by co-precipitation with the As (or P). The yellowish and reddish layers were also clearly resolved by both Mössbauer spectroscopy and magnetometry. Complexation of arsenate onto the HFO core was found to significantly increase the average quadrupole splitting (QS) obtained from Mössbauer spectroscopy by an amount that could not be explained by other chemical differences and that is consistent with an ~1 nm diameter particle size and somewhat smaller HFO core. The Munsell hue YR index (5–10 YR) was found to be strongly correlated to the average QS, thereby establishing that the color differences, corresponding to the measured shifts of the main visible band edge, are due to the local distortions in the $^{[6]}Fe^{3+}$ environments that are induced by As complexation, via their influence on the relevant ligand field transitions. SQUID magnetometry allows the following observations. (1) The superparamagnetic to superferromagnetic transitions occur at 25 K and lower in As-HFO, compared to 55 K in synthetic 2-line ferrihydrite, suggesting a smaller magnetic primary particle (or core) size for As-HFO and inter-particle magnetic interaction reduction by surface complexed As, Si, and C. (2) The ratio of supermoment magnitude to magnetic particle size (m^2/n, where m is the net number of Fe^{3+} atomic moments per supermoment and n is the number of Fe^{3+} cations per particle or HFO core) decreases with increasing As content in the sequence synthetic-HFO > reddish-As-HFO > yellowish-As-HFO. (3) The magnetic susceptibility magnitudes for As-HFO and synthetic 2-line ferrihydrite differ by a factor of 10 and suggest different supermoment formation mechanisms ($m^2/n < 1$ vs. $m^2/n > 1$, respectively) related to differences in intra-particle cationic and anionic disorder and magnetic particle size.

* E-mail: dgr@physics.uottawa.ca
† Present address: Department of Geology, University of South Florida, Tampa, Florida 33620, U.S.A.

INTRODUCTION

The mobility and immobilization of As in natural waters is, in most circumstances, controlled by sorption onto particulate phases (Mok and Wai 1994). In particular, hydrous ferric oxide (HFO) is known to have a great sorption affinity for both arsenite [As(III)] and arsenate [As(V)] and sorption onto HFO is believed to be a dominant mechanism controlling As cycling in many natural environments (Cullen and Reimer 1989; Maher and Butler 1988). Dominant As/HFO associations have been documented (or inferred) to occur in: lacustrine sediments (e.g., Aggett and O'Brian 1985; Belzile and Tessier 1990; Peterson and Carpenter 1986), marine sediments (e.g., Belzile 1988; Edenborn et al. 1986), soils (e.g., Hess and Blanchar 1976; Bowell 1994) and acid mine drainage environments (e.g., Leblanc et al. 1996). In addition, sorption onto HFO is believed to be the main mechanism in the common ferric chloride coagulant-based water treatment method for As removal (Hering et al. 1996, 1997) and the most effective As removal treatment of spent hydrothermal fluid in hydrothermal power generation plants has been found to be As/HFO coprecipitation combined with a standard flotation separation (De Carlo and Thomas 1985).

The arsenic forms associated with solid phases in aquatic sediments and their role in the biogeochemical cycling of As are largely unknown, at least partly because the relevant mineralogy has been mostly inferred from indirect measurements such as porewater concentrations of dissolved species and selective chemical dissolution of the solid sediment (Cullen and Reimer 1989; Maher 1984; Maher and Butler 1988; Woolson 1977). The precise mineralogy and crystal chemistry of these forms may play a significant role in determining bioavailability for many organisms (Lee et al. 2000; Maher 1984). In addition, environmental As/HFO materials are expected to be very similar (same column in the periodic table) in structure and chemistry to environmental P/HFO materials that are believed to play a dominant role in P cycles (Parfitt 1978), yet are easier to characterize by many physical methods that are sensitive to atomic mass (diffraction in particular). Greater knowledge of the precise mineralogy of key reactive phases (e.g., P/HFO and heavy metal HFO associations), in turn, would allow advanced reaction transport models of sediment diagenesis to be further developed (Van Cappellen and Wang 1996). Finally, As/HFO coprecipitation probably represents the main route of As removal from hydrothermal fluids and deposition to the sea floor, which is by far the largest geochemical reservoir of As (Maher and Butler 1988). These are some of the many reasons to obtain detailed mineralogical characterizations of natural As/HFO materials, that have motivated the present study.

Because of the importance of As/HFO associations in both natural and anthropogenic settings, there have been several detailed mineralogical studies of synthetic As-HFO sorbate-sorbant materials and coprecipitates (Raven et al. 1998; Wilkie and Hering 1996; Waychunas et al. 1996, 1995, 1993; Manceau 1995; Rea et al. 1994; Fuller et al. 1993; Pierce and Moore 1982). These studies have demonstrated the large As sorption capacity of HFO, showing that sorption densities as high as 0.7 and 0.25 mole-As/mole-Fe can be obtained in coprecipitation and sorption experiments, respectively (Fuller et al. 1993). Such demonstrated capacity far exceeds current technological limits using other sorbants, such as "granular ferric hydroxide" (a Cl-bearing poorly crystallized β-FeOOH compound resembling akaganéite) which attains 0.06 mole-As/mole-Fe (Driehaus et al. 1998). The large demonstrated As sorption densities suggest that the As-HFO materials are intermediate between classic sorbate-sorbant systems and solid solutions or compounds in which the As and Fe occupy cation sites in a crystal structure that is more stable than a two-phase mixture. Indeed, the As is found to stabilize the HFO with respect to transformations to other oxides and to complex to the HFO surface in such a way as to modify the local coordination environments of a significant fraction of the Fe (Waychunas et al. 1996). The large sorption densities can be partly understood by the intrinsic nanocrystalline nature of 2-line ferrihydrite (typically 1–3 nm diameters) but the large values occurring in coprecipitation probably involve significantly smaller HFO particles (or less densely packed primary HFO particles) whose growth (or agglomeration) is poisoned by As complexation.

In this paper, we report a mineralogical characterization of the most As-rich (by two orders of magnitude) natural HFO precipitates ever described, that attain sorption densities of ~0.1–0.2 mole-As/mole-Fe. These As-sorbed HFO materials were formed by rapid abiotic precipitation when an As and Fe^{2+}-rich hydrothermal fluid mixed with seawater, thereby preventing otherwise certain destruction of the surrounding coral reef ecosystem (Pichler et al. 1999a; Pichler and Veizer 1999; Pichler 1998).

Note that we follow current practice (Cornell and Schwertmann 1996) by reserving the term "2-line ferrihydrite" for the HFO material that has the corresponding characteristic powder X-ray diffraction (pXRD) pattern consisting of two well defined Bragg peaks. We use the term HFO for all 2-line ferrihydrite-like materials, including: (1) 2-line ferrihydrite itself, both in cases where it was identified as such and in cases where it is inferred to be 2-line ferrihydrite although the pXRD pattern was not measured; (2) materials that are less crystalline (or have smaller particle sizes) than 2-line ferrihydrite and that consequently have pXRD patterns that either do not have any pXRD peaks or have significantly broadened ones; and (3) sorbed or coprecipitated 2-line ferrihydrite-like materials having pXRD patterns that are qualitatively the same but may be significantly different in shape from the characteristic pXRD pattern of 2-line ferrihydrite. We take HFO materials to exclude the more crystalline ferrihydrite varieties (3-line to 6-line ferrihydrite).

SAMPLE PROVENANCE AND GEOLOGICAL SETTING

The collection area lies along the southwest margin of Ambitle Island (4°05'S, 153°40'W), one of the Feni islands in the southernmost island group of the Tabar-Feni chain, off the coast of Papua New Guinea. The island is part of a Quaternary stratovolcano with a central eroded caldera built on poorly exposed Oligocene marine limestone (Wallace et al. 1983). Volcanic strata (interbedded lava flows, lahar deposits, tuffs, and scoriae) dip radially from the island, presumably extending

beneath the shelf. Several geothermal areas are located primarily along the western coast and in the western part of the caldera near breaches in the caldera wall.

Submarine hydrothermal venting occurs at Tutum Bay in shallow (5–10 m) water along the inner shelf that contains a patchy distribution of coral-algal reefs surrounded by medium to coarse-grained mixed carbonate-volcaniclastic sand and gravel (Pichler and Dix 1996). Two types of venting are observed: (1) focused discharge of a clear hydrothermal fluid occurs at discrete ports, 10–15 cm in diameter, where fluid temperatures at vent orifices are between 89 and 98 °C and (2) dispersed or diffuse discharge consisting of streams of gas bubbles emerging directly through the sandy to pebbly unconsolidated sediment and through fractures in volcanic rocks. A more detailed description of Tutum Bay is provided elsewhere (Pichler and Dix 1996; Pichler et al. 1999b) and color images can be found at http://chuma.cas.usf.edu/~pichler/.

As-bearing HFO materials are present throughout Tutum Bay where they form as thin layers on sediment grains in areas of high sea floor temperatures. Massive layers and extensive filling of sediment pore space also occurs but is restricted to the vicinity of vent sites where the HFO materials form bright orange coatings on volcanic boulders, distinct bands on coral skeletons and aragonite, and/or precipitate as massive layers in open spaces. The HFO precipitation at these vent sites has been studied by thermodynamic modeling and is found to occur as expected from such models, given the measured local physical and chemical conditions (Pichler 1998; Pichler and Veizer 1999; Pichler et al. 1999b). The HFO materials vary in color from a bright orange to a very dark brown that is almost black and have hardnesses, on Mohs' hardness scale, from less than 1 to ~2.5. Banding into ~0.1–10 mm thick layers that are mostly parallel to the substrate surface and that have distinct color differences (predominantly yellowish vs. predominantly reddish) is common on all substrates. All samples were found to be stable in air after collection and were simply washed with deionized water and left to dry at room temperature before the various measurements were applied.

The samples studied in the present work are described in Table 1, in which their dry powder colors are described using the Munsell soil color chart system. Included are four relatively pure As-HFO samples (V2AR, V2BY, 97R, and 97Y) and one sample (FV1) that contained significant amounts of other mineral phases and that illustrates the evolution of the As-HFO materials toward other more stable Fe-bearing and As-bearing phases. Samples V2AR and 97R show intermediate degrees of evolution, with some crystalline phases being present. Such evolution has been described elsewhere and several more samples were studied by chemical analyses (Pichler 1998). Samples V2AR and V2BY are from the two main and adjacent layers (reddish and yellowish, respectively) that make up one deposit, as are samples 97R and 97Y (Table 1). These couplets (V2AR/V2BY and 97R/97Y) were chosen in an attempt to quantify the physical and chemical differences that give rise to the color banding, as a first step in studying its mechanism and role in the overall aging of the samples. Note that the yellowish and reddish bands occur in reversed order in the two couplets (Table 1). This may arise from the fact that the V2AR/V2BY couplet was in contact with seawater relatively far away from the vent, whereas the 97R/97Y couplet was directly exposed to the mixing hydrothermal fluid for some time (Table 1).

Experimental and analysis methods

For transmission electron microscopy (TEM), dry samples were finely crushed in a glass mortar and dispersed in LR White embedding resin. Samples were twice infiltrated with the resin for 60 minutes before being re-suspended in fresh resin and polymerized at 60 °C for one hour. Thin sections (80–90 nm) were cut with a diamond knife mounted onto an ultramicrotome and collected on carbon coated Ni-grids having a supporting Formvar film. The thin sections were observed with a Philips EM400T electron microscope equipped with an X-ray spectrometer (LinK Analytical eXL/LZ-5) for elemental analysis. Energy dispersive spectroscopy (EDS) was performed at 100 kV with a beam current of 10 nA for ~100 seconds (live time). The size of the electron beam was 100 nm. Selected area electron diffraction (SAED) analyses were performed at 100 kV and the camera constant value was 640 nm.

The pXRD patterns were collected using an automated Philips X'Pert PW3710 system θ–2θ powder diffractometer, using Cu$K\alpha$ radiation with a variable divergent slit and a solid state detector. Samples were mounted as acetone smears on a single-crystal Si wafer low-background holder that spun during data collection. The low-background holder gave a struc-

Table 1. Description of the natural As-HFO samples

Sample	Location*	Description†
FV1	Vent-1	Massive layers (several cm thick) with alternating colors (banding) ranging from dark brown to dark orange, indurated and relatively hard compared to the other As-HFO samples. The dried and powdered sample studied had Munsell color "yellowish red" wish hue/value/chroma = 5YR 4/6.‡
V2AR,V2BY	Vent-2	Massive deposit of As-HFO (~6 mm thick), on dead coral fragments and aragonite, consisting of two layers (each ~3 mm thick): V2AR is reddish brown (Munsell "strong brown," hue/value/chroma = 7.5YR 5/8, dry powdered sample) and relatively hard whereas V2BY is yellowish brown (Munsell "brownish yellow," 10YR 6/6) and relatively soft. V2BY is beneath the V2AR layer and in closer contact with the coral substrate whereas V2AR is on top of the V2BY layer and in direct contact with sea water.
97R, 97Y	Vent-4	Very soft As-HFO materials collected from a coral skeleton that had partly fallen over the vent orifice, from the side of the skeleton that faced the vent. 97Y is yellowish (Munsell "yellowish brown," 10YR 5/6) whereas 97R is reddish (Munsell "reddish brown," 5YR 4/4). The two materials are in layers of ~3 mm average thickness, ~3 cm maximum thickness. In this case, the 97Y layer was in closer contact with the coral skeleton and was shielded from contact with the hydrothermal fluid and seawater by the 97Y layer (reversed relative to the V2AR/V2BY couplet).

* Pichler (1998).
† All Munsell determinations were done on dry powdered samples.
‡ Our synthetic HFO comparison materials had Munsell: hue = 2.5YR, value = 2.5, and chroma in the range 1–3.

tureless background that cannot mask or interfere with the broad lines arising from the samples, in the entire 2θ range of interest. Tests showed that control smears with only acetone also gave no detectable signals that could interfere with the signals from the samples. For pXRD and most measurements (vis-IR, Mössbauer, Munsell color determination, magnetometry, GC) the samples were not ground extensively but were powdered by simple tapping of dry pieces between sheets of wax paper, using a scalpel handle, in order to subject them to the least amount of mechanical treatment.

Room temperature (*RT* = 22 °C) ^{57}Fe Mössbauer spectra were collected in transmission mode using random orientation powder absorbers having 27–41 mg of dry sample per cm^2 in holders with 1/2 inch diameter windows. Calibration was obtained using an enriched ^{57}Fe foil at *RT* and all center shifts (CSs) are reported with respect to the CS of metallic iron at *RT*. The transducer was operated in constant acceleration mode and folding was performed to achieve a flat background. All Mössbauer spectra were fit with the Voigt-based fitting method of Rancourt and Ping (1991) for quadrupole splitting distributions (QSDs), using the Recoil software of Lagarec and Rancourt (http://www.physics.uottawa.ca/~recoil/). Please consult the original article of Rancourt and Ping (1991) for all Mössbauer parameter definitions and a description of the relevant notation. All measurements were performed with a velocity range of ±11 mm/s and several measurements were performed on an expanded velocity range of ±4 mm/s. The larger range allowed possible detection of magnetically split patterns from bulk Fe oxides whereas the smaller range gave an optimal resolution for the As-HFO pattern. Fitting results for the two velocity ranges for a given sample were identical within statistical errors of the fitting parameters. Liquid nitrogen temperature (*LNT* = 77 K) spectra were collected and calibrated in a similar way, in a cryostat in which the source was also maintained at *T* = 77 K. As a result the CSs of the *LNT* spectra are shifted by an amount equal to the second order Doppler shift (SOD) of the source, that is, by the difference in SOD in going from *RT* to *LNT* [must add 0.12(1) mm/s to quoted *LNT* CS values].

The SQUID magnetometry measurements were performed on a low-field dc SQUID magnetometer that has been described elsewhere (Lamarche 1989). Typically a few milligrams of powder sample were immobilized in the cryogenic holder. The sample was first zero-field quenched (Earth's field), then the field was turned on (typically 40–70 Gauss) and the magnetic moment on the sample was measured on warming (field warming, FW). After the maximum temperature was reached or at some other chosen temperature, one could choose to measure as the sample was recooled (field cooling, FC). The following field strengths were used for the various samples: 72.2 Gauss, samples 97R and 97Y, 52.2 Gauss, samples V2AR and V2BY; and 39.8, 40.7, and 40.0 Gauss for HFO samples synthesized with pH = 9, 7, and 6, respectively ([Fe] = 10^{-3} *M*).

Diffuse reflectivity spectra (vis-IR = 350–2100 nm) were obtained at *RT* with a Cary-14 spectrophotometer configured with a 23 cm diameter integrating sphere. The instrument has a double-beam double monochromator with a resolving power of 0.1–0.3 nm and a wavelength accuracy of ~0.4 nm. Sample and reference ports are located in the bottom of the sphere so that samples are measured in a horizontal orientation flush with port openings. Beam size (monochromatic light) at sample and reference ports was ~1.0 × 2.0 cm. Halon is used as the reflectivity standard and as the coating for the integrating sphere. Reflectivity measurements were converted to absolute reflectivity using literature data for the absolute reflectivity of Halon (Weidner and Hsia 1981). The compartment of the Cary-14 that contains the integrating sphere and samples was flushed with dry N_2 gas (derived from liquid N_2) for at least 1 hour prior to obtaining reflectivity spectra. Reported spectra are the average of three scans, and the intensity of the bands at 1400 and 1900 nm, that result from H_2O and OH, did not change during measurement. Because of limited amounts of sample (~25 to 160 mg), sample thickness was 0.012–0.080 g/cm^2 in sample cups that were Al metal painted with optically black paint. Assuming a powder density of 2.0 g/cm^3, sample thickness is 0.06–0.40 mm. The work of Buckingham and Sommer (1983) suggests that a thickness of 0.025 mm is sufficient for conditions of effectively infinite thickness (i.e., incident light did not see the sample cup) for fine-grained powders of iron oxides.

XRF elemental analyses were obtained using a Philips PW2400/00 Sequential X-ray Spectrometer. Because of limited sample amounts (given the self-imposed constraint of using exactly the same sample fractions for all measurements), a special calibration was developed in which fused disks were prepared using only 20 mg of sample for 4.0750 g of flux material (3.2000 g $Li_2B_4O_7$; 0.8750 g $LiBO_2$). The calibration was for the eight most abundant elements excluding As. Extensive tests that involved repeated measurements on a given fused disk and comparisons with relevant standards that were not used in establishing the calibration allowed us to conclude that the accuracy of the measurement for the eight calibrated elements (Fe, Si, Na, Ca, Al, Mg, P, and K) was ~1 wt% and that the precision was ~0.1 wt%. The measured loss on ignition (LOI) of a given sample had an accuracy of ~3 wt% that was mainly determined by the uncertainty in weight loss of the flux, that is ~0.01 wt%. Arsenic was treated in a separate way, because of the difficulty in obtaining As-rich standards as fused disks. Background-corrected fluorescence peak counts were calibrated against a fused disk made using a synthetic Fe-As compound. The resulting accuracy in As is estimated at ~5%, including both uncertainties in the synthetic standard and systematic errors from not fully including matrix effects, whereas the comparative (sample to sample) precision is much better (~0.1%). The latter number is from the statistical error on the total number of background corrected counts for the given fluorescence peak. The magnitudes of As amounts found are in fair agreement with values for similar samples, obtained from neutron activation measurements (Pichler 1998).

Light element analyses (C, H, N, S) were obtained by gas chromatography (GC) of combustion products using thermal conductivity (thermistor) detection with a CE Instruments model EA-1110 elemental analyzer. Quantification was achieved by using time-integrated thermistor signals and corresponding run-specific calibrations for C, H, N, and S. Several standards were run before, during, and after the

measurements, that were used to construct a linear calibration curve for each element. Detection limit and accuracy are ~0.01 wt% of the element.

Synthetic 2-line ferrihydrite reference material

In order to correctly characterize our natural As-HFO samples and to elucidate the role of As in its crystal chemical structure and microstructure, it is important to have a relevant comparison point. The obvious choice is pure synthetic 2-line ferrihydrite, which is also formed by rapid precipitation and is believed to be the best candidate to model the sorbant phase of As-HFO, in a sorbate-sorbant picture.

In another study (unpublished) we have synthesized and extensively characterized several synthetic 2-line ferrihydrite samples, formed by rapid oxidation and precipitation of Fe^{2+}, at pH values of 6, 7, 8, and 9, and at initial Fe concentrations of both 10^{-3} or 10^{-4} *M*. In all cases, except at [Fe] = 10^{-3} *M* and pH = 8 where a mixture of lepidocrocite and goethite resulted, pure 2-line ferrihydrite was produced. The precipitates were washed with ultrapure water and freeze dried prior to measurements. All these synthetic ferrihydrite samples had measured characteristics (pXRD, Mössbauer spectra, TEM, compositions) similar to those for both natural and synthetic 2-line ferrihydrite (Jambor and Dutrizac 1998; Cornell and Schwertmann 1996; Childs 1992). They had variations of their characteristics on synthesis conditions (pH and [Fe]) that were much smaller than the differences in characteristics between any such synthetic or natural 2-line ferrihydrite sample and our As-HFO materials.

Therefore, although 2-line ferrihydrite is itself a complex material whose structure, microstructure, and crystal chemistry are far from well known (notwithstanding a recent high resolution TEM study that is of special note in this regard: Janney et al. 2000), it can be reproducibly synthesized and unambiguously identified. It also has sufficiently narrow spreads in measured characteristics, from one 2-line ferrihydrite sample to another, to make it an appropriate reference material for comparisons with its various sorbed, coprecipitated, or cation substituted varieties. Regarding Mössbauer spectroscopy, this is corroborated by a complete literature review of the *RT* parameters (CS and average QS) of natural and synthetic As-poor and As-free HFO materials (Thibault 2001). The latter study shows that the distributions of sample-specific average QS values for natural and synthetic samples are almost indistinguishable: mean = 0.75(2) mm/s, standard deviation = 0.062 mm/s, for natural samples (n = 10), compared to mean = 0.707(8) mm/s, standard deviation = 0.047 mm/s, for synthetic samples (n = 36), obtained from Lorentzian doublet fits. Both values of the mean are much smaller than typical values found for As-HFO samples. The slightly larger values of the mean and standard deviation for the natural samples may be due to the natural samples having various compositional differences, although the difference is small given the large variation in Si contents.

Indeed, a main complicating factor is the mostly unknown effects of Si in natural ferrihydrite materials, since our As-HFO samples do contain significant amounts of SiO_2. We expect the contribution from the effects of Si in our As-HFO samples to be small because unambiguous and systematic effects of Si on pXRD patterns and *RT* Mössbauer spectra of natural and synthetic ferrihydrite materials, with widely different Si/Fe ratios, have not been reported (Jambor and Dutrizac 1998; Childs 1992), except recently (e.g., Zhao et al. 1996; Glasauer et al. 2000). The latter authors convincingly argue that Si does not enter the HFO structure but instead complexes to the surfaces of HFO primary particles. Several results in the present study suggest that the same is true for As and that As and Si (or C) compete for reactive sites on HFO cores. In cases where authors report Si entering the HFO structure (e.g., Boyd and Scott 1999), the effects seen can also be attributed to other sample characteristics and they are small compared to the differences between As-HFO and As-free HFO reported here. In particular, the pXRD patterns of Si-rich HFO samples are not significantly different from those of Si-poor samples (Glasauer et al. 2000).

Results and discussion

Powder X-ray diffraction

The pXRD patterns are shown in Figure 1 where they are compared to the pXRD pattern of a synthetic 2-line ferrihydrite ([Fe] = 10^{-3} *M*, pH = 9). Sample FV1 (Table 1) is an example of a presumably older deposit in which the As-HFO has largely transformed to a possibly As-bearing 6-line ferrihydrite, with its six main diffraction peaks labeled F, that coexists with several crystalline phases that give rise to prominent Bragg peaks that are labeled as follows: S for a smectite-illite mixture, B for bassanite ($CaSO_4 \cdot 0.5H_2O$), and C for claudetite (As_2O_3). It is likely that all samples are predominantly As-HFO when freshly precipitated and that the solid phase composition of FV1 has arisen by aging in contact with seawater (e.g., Pichler 1998). In addition to bassanite, anhydrite ($CaSO_4$) was detected in one diffractogram of sample 97R where it may have resulted from post collection dehydration of a small amount of bassanite. The formation of bassanite (in FV1) is consistent with the known behavior of the aqueous $CaSO_4$-H_2O system, in the presence of NaCl and at the observed elevated sea floor temperatures (Deer et al. 1966). This would explain the relative hardness of FV1 (Table 1) in terms of filing of sediment pore space by authegenic bassanite.

The reddish samples (V2AR and 97R) are predominantly As-HFO and contain small amounts of smectite-illite mixtures and claudetite. The yellowish samples (V2BY and 97Y) are predominantly As-HFO with no detectable amounts of other solid phases, except for halite (NaCl) that appears in some diffractograms and that is probably produced from residual seawater during drying. That the amounts of crystalline phases in the reddish samples (V2AR and 97R) are small is clear from: (1) reference intensity ratio calculations applied to the diffraction peaks; (2) our TEM investigation of the same samples (described below); and (3) our bulk chemical analyses (e.g., total Ca, described below). Nonetheless, the reddish samples seem to have been more susceptible than the yellowish samples to the type of aging that presumably has occurred in FV1. The initial aging sequence appears to be from As-HFO (2-line As-

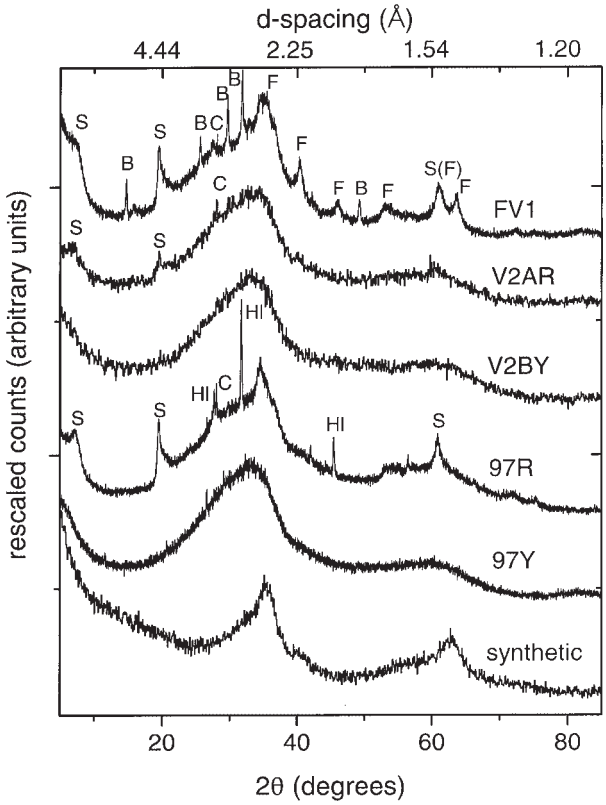

FIGURE 1. Powder X-ray diffraction patterns of As-HFO samples FV1, V2AR, V2BY, 97R, and 97Y (as indicated), compared to the pXRD pattern of a synthetic HFO sample ([Fe] = 10^{-3} *M*, pH = 9). The synthetic sample exhibits the pXRD pattern of a classic 2-line ferrihydrite material. Sample FV1 largely consists of a 6-line ferrihydrite having its six main peaks labeled F and contains small amounts of other crystalline phases having main peaks labeled S for a smectite-illite mixture, B for bassanite, and C for claudetite. The reddish As-HFO samples (V2AR and 97R) contain small amounts of smectite-illite and claudetite, as labeled. Halite (NaCl, labeled Hl) from residual sea water occurred in several diffractograms.

bearing HFO) to less As-rich 6-line ferrihydrite with excess Si and some Fe forming a smectite-illite mixture and excess As forming claudetite, accompanied by consolidation via authigenic bassanite. Smectite-illite mixtures are common in hydrothermal environments (e.g., Ylagan et al. 2000) and these T-O-T type layer silicate mixtures may initially form from the Fe^{3+} layered octahedra of HFO having tetrahedral Si^{4+} complexed to their faces. The 2-line to 6-line evolution of the predominant As-HFO component is unusual in that such evolution has not been reported in other natural environments (Cornell and Schwertmann 1996) and may be made possible in part by the elevated sea floor temperatures in our case. In terrestrial surface environments and in related laboratory experiments HFO evolves directly to hematite or goethite (Cornell and Schwertmann 1996).

Overall, on first examination, the pXRD patterns of the As-HFO samples (Fig. 1) show two very broad Bragg humps at *d* spacings of approximately 1.5 and 2.5 Å which are generally taken to be characteristic of 2-line ferrihydrite (thus the name). This might bring one to conclude that the samples are simply 2-line ferrihydrite. In fact, more information can be derived from the pXRD patterns. Such pXRD patterns are directly related to the underlying radial distribution functions (i.e., angle-averaged Patterson functions that include all disorder and finite particle size effects), as is well known in the study of amorphous materials and liquids. This means that the differences in pXRD pattern shapes translate into differences in populations of cation-cation, cation-anion, and to a lesser extent anion-anion distances. This was used by Waychunas et al. (1996) to study synthetic As-HFO materials, in comparison with extended X-ray absorption fine structure (EXAFS) results. In light of the latter study, the systematic differences in the 1.5 and 2.5 Å peaks of our As-HFO samples and 2-line ferrihydrite (Fig. 2), consisting in more intensity on the high *d* spacing sides of the As-HFO peaks, can be interpreted as being due to a significant population of Fe-As structural pairs, across shared bridging coordination O anions on the surface (Waychunas et al. 1996). The presence of a significant population of nearest neighbor As-O pairs can also be inferred and the general smearing out (broadening), relative to the Bragg peaks of 2-line ferrihydrite, is understood in terms of smaller X-ray coherent domains (i.e., smaller primary particles) in the As-HFO materials.

One concludes from the pXRD measurements (Figs. 1 and 2) that our As-HFO materials are significantly different from As-free 2-line ferrihydrite and that they have patterns like those of synthetic As-HFO samples (Waychunas et al. 1996). The As is not in a separate crystalline phase (the very small amounts of claudetite in the reddish samples notwithstanding) and there is evidence for Fe-As pairs that precludes most of the As from being in separate amorphous or nanocrystalline phases. The pXRD patterns are correlated to sample color in that the reddish samples have small amounts of secondary phases but the latter secondary phases (mainly smectite-illite) would be ex-

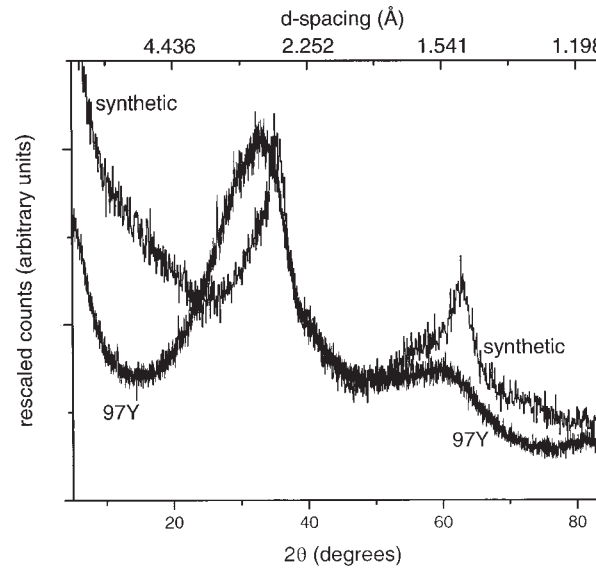

FIGURE 2. Detailed comparison of the pXRD patterns of As-HFO sample 97Y and a synthetic HFO sample ([Fe] = 10^{-3} *M*, pH = 9). The data has been rescaled and shifted in order to facilitate comparison. This allows a detailed comparison between pure synthetic 2-line ferrihydrite (HFO) and pure (Si- and C-bearing) As-HFO.

pected to make the samples less red by reducing the relative amounts of iron oxyhydroxides. The yellowish color must be attributed to As complexation in As-HFO, in samples (V2BY and 97Y) that do not contain detectable secondary phases, as corroborated by several other measurements described below.

Transmission electron microscopy

TEM micrographs for samples 97Y and 97R are shown in Figure 3. Such micrographs, combined with extensive TEM-based SAED and EDS measurements, allow us to conclude: (1) that there is no evidence for separate phases on this size scale or for phases other than the predominant As-HFO seen by pXRD; (2) that there is no evidence for bacteria or associated biologically induced mineralization, which is common in other hydrothermal vent environments (Fortin et al. 1998; Rona 1988; Juniper and Fouquet 1988); and (3) that the As-HFO particles are agglomerated into large spheroidal objects having typical dimensions 100–1000 nm. Chemical analyses for samples 97Y and 97R based on an average of seven EDS probe spots, in areas where the beam size was smaller than the sample structure, are given in Table 2 as elemental ratios, where they are compared to the bulk XRF values for all As-HFO samples. The TEM-based EDS analyses are semiquantitative in that we expect particle morphology and differences in compactness to significantly affect the results.

Samples 97Y and 97R display somewhat different submicrometer-scale morphologies (Fig. 3), with spheroidal and elongated agglomerations typically having dimensions 150–250 nm (diameters of spheroids), 200 × 300 nm, 400 × 500 nm, and 600 × 1000 nm in 97Y and 100–150 nm (diameters of spheroids) and 150 × 350 nm in 97R. The agglomerations are composed of nanometer-scale As-HFO particles that are detected as dense spots in Figure 3 (arrows) and that are typical of ferrihydrite particles seen at this magnification.

Chemical analyses: XRF and GC

The XRF results are reported as weight fractions of the assumed oxides in Table 3. The XRF method does not suffer from problems related to sample non-homogeneity on the scale of the sub-sample to be measured because it is based on a fused disk approach in which the non-volatile elements are uniformly dispersed. In the case of sample 97Y, there was enough material to perform five measurements, on separate fused disks. The sub-sample to sub-sample variations (97Y, Table 3) are larger than the accuracy and precision and are interpreted as arising from the combined effects of: (1) true sub-sample variations due to sample inhomogeneity, and (2) possible fusing problems related to As and As-Fe interactions. The large values for the total weight may be partly due to a systematic over estimation of the As, arising from the incomplete matrix effects corrections for this element but that does not negatively affect comparative precision. The LOI is interpreted as corresponding to total OH + H_2O, including both sorbed and tightly bonded water. The loss of OH groups is not an oxidation since it is not expected to be associated with a change of ionization state of the structural cations. It is expected to occur as $2Fe(OH)_3 = Fe_2O_3 + 3H_2O$ or as $2OH^- = O^{2-} + H_2O$, such that the weight of $1/2H_2O$ is lost for every H removed from the structure, as is also the case for desorbed molecular water. Therefore, LOI can be taken to be related to total H as $m_H = 2(LOI/M_{H_2O})$, where M_{H_2O} is the molar mass of water and m_H is the number of moles of H per 100 wt% of sample. Table 4 shows that the latter calculated total H agrees well with the total H directly measured by GC, thereby corroborating this interpretation of the LOI, within our accuracy limits.

The XRF results (Table 3) clearly demonstrate a systematic difference between the reddish samples (97R and V2AR) and the associated yellowish samples (97Y and V2BY, respectively) in which the reddish samples have: less Fe_2O_3, less As_2O_5, and more SiO_2. This translates (Table 2) into the reddish samples having significantly smaller As/Fe and larger Si/Fe ratios. These differences are not seen by the TEM-based EDS method because of its semiquantitative nature with such samples. Such systematic compositional differences between reddish and yellowish As-HFO samples from this geothermal area have not previously been reported but they are real. They are also important, as they give a chemical basis for the observed differences in color and other physical properties, such as the susceptibility to smectite-illite formation described above and the Mössbauer parameters and magnetism described below. They suggest that there is competition between As and Si for surface complexation to HFO. A similar competition, between P and Si, has been observed in sorption/desorption experiments with ferrihydrite (Parfitt 1989) and another similar competition, between C (as sorbed onto HFO from natural organic matter) and As, was observed in a study of As removal from drinking water (Hering et al. 1997).

The only other example that we are aware of where As-HFO material forms banded structures with alternating reddish and yellowish layers is the case described by Leblanc et al. (1996) of ferruginous accretions produced in an acid mine water environment. The latter material is similar to our samples in many respects. Their As contents and layer thicknesses are comparable to ours and, as is the case with our samples, the reddish layers are harder, have more advanced crystallization to more stable phases, and contain significantly less As. Their materials, however, do not contain significant amounts of Si.

Apart from the red/yellow differences, the chemical analysis results (Tables 2 and 3) are in general agreement with previous evaluations on related samples (Pichler 1998; Pichler and Veizer 1999; Pichler et al. 1999a) and show the samples to be very As-rich (0.1–0.2 mole As/mole Fe) but to otherwise be similar to natural As-free ferrihydrite samples (Jambor and Dutrizac 1998), in their Si and minor element contents and in their LOI values. Natural and synthetic (Saleh and Jones 1984; Vempati et al. 1990) ferrihydrite samples can typically contain such large Si/Fe ratios as those found in our As-HFO samples. There have been no systematic studies of the effect of Si on the pXRD patterns of 2-line ferrihydrite samples and there also have been no conclusive reports that Si has a systematic effect on the pXRD patterns of ferrihydrite samples of any type (Jambor and Dutrizac 1998). Indeed, many Si-rich 2-line ferrihydrite samples are found to have pXRD that are not significantly different from those of Si-poor 2-line ferrihydrite samples (e.g., Glasauer et al. 2000; their Fig. 1 compared to our Figs. 1 and 2). Also, the large differences in SiO_2 contents

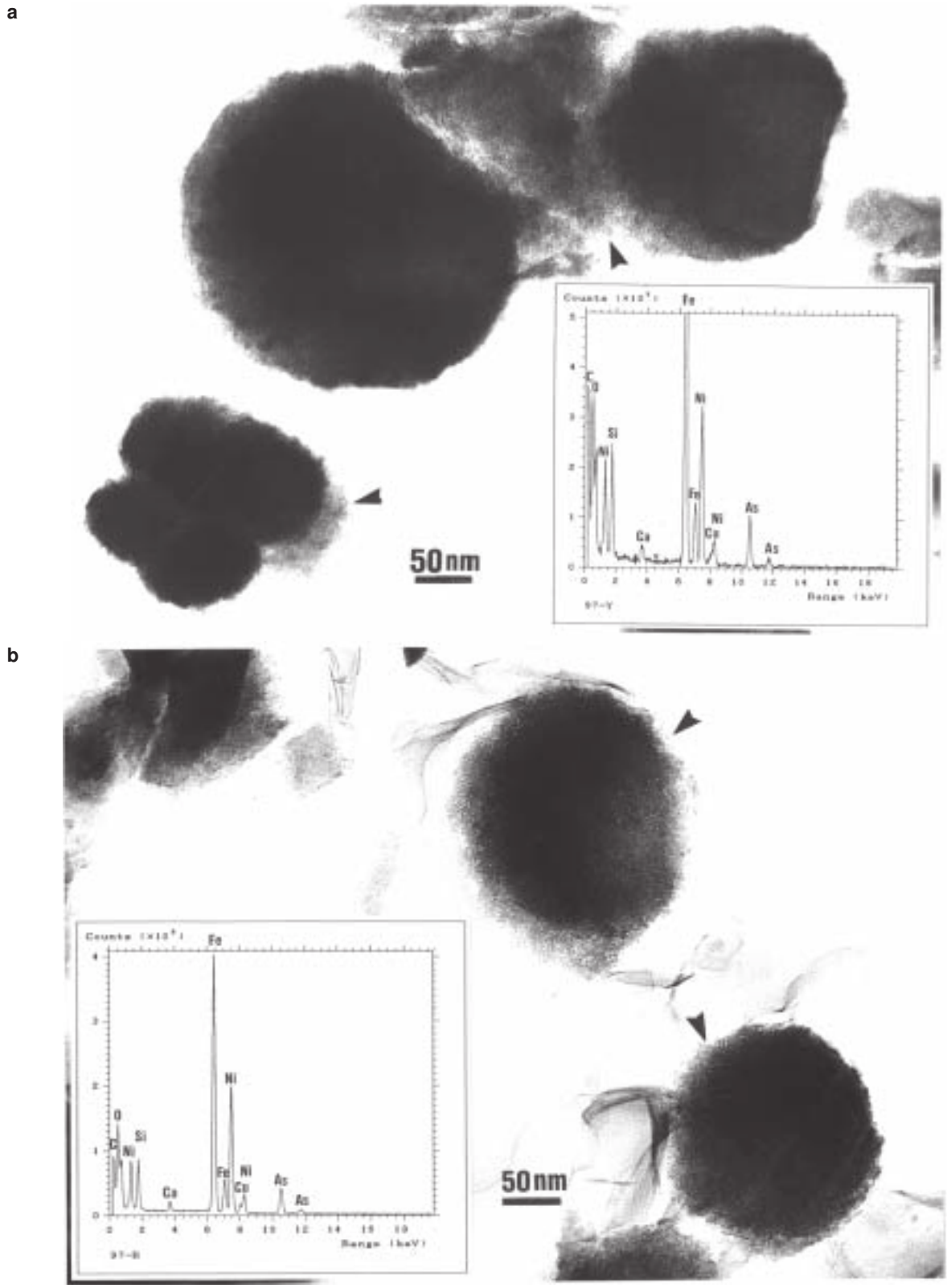

FIGURE 3. TEM thin-section micrographs and sample EDS spectra for As-HFO samples: (**a**) 97Y and (**b**) 97R. The arrows point to examples of primary particles, that are seen as dark ~1–5 nm spots at this magnification. The Ni in the EDS spectra is from the Ni grid sample supports that are used. The Cu*K*α line has an interference with the Ni*K*β line, such that Cu cannot reliably be quantified but in any case occurs in relatively small amount.

TABLE 2. Molar ratios from TEM-based EDS analyses for 97R and 97Y, compared to values from XRF analyses

Sample	As/Fe	Si/Fe	Ca/Fe
97R	0.13	0.26	0.035
97Y	0.12	0.34	0.034
97R*	0.18	0.44	0.055
97Y	0.26	0.17	0.047
V2AR	0.14	0.33	0.057
V2BY	0.22	0.22	0.053
FV1	0.15	0.31	0.039

* Using only 97R-1 from Table 3, because 97R-2 seems anomalous in both As and LOI.

TABLE 4. GC results: Light element analysis*

Sample	C (wt%)	C/Fe	H (wt%)	H/Fe	H/Fe†
97R	1.84	0.24	2.05	3.1	3.7
97Y	0.97	0.12	1.90	2.6	2.4
V2AR	2.65	0.34	2.10	3.2	3.0
V2BY	1.43	0.16	1.84	2.5	2.5
syn-HFO‡	0.18	0.01	1.79	1.67	1.45

* A detected N signal is near the detection limit. There is no detected S.
† Calculated using LOI (from XRF fusions), as H = (LOI/M_{H_2O}) × 2.
‡ pH = 7; [Fe] = 10^{-3} *M*; freeze dried.

reported in Tables 2 and 3 do not have any detectable systematic effect on the measured pXRD patterns, apart from the observed different susceptibilities to form (Si-bearing) smectite-illite phases and claudetite (Fig. 1). For these reasons, and because Si has a smaller atomic number than Fe and As, we did not consider the presence of Si in our above interpretation of the pXRD results. The same holds for the presence of C, that we have quantified by GC as described below.

The GC light element analysis results are given in Table 4. It is interesting to note a significant amount of C that is correlated to sample color in the same way as Si (Table 2). The reddish samples (97R and V2AR) have approximately twice as much C as their yellowish counterparts (97Y and V2BY, respectively). This C is probably not organic (TEM results) and may be complexed to the HFO surfaces in much the same way as the Si. As noted above, the measured H contents allow a quantitative interpretation of the measured LOI, that also holds for synthetic HFO. Interestingly, the weight fractions of H for As-HFO and for synthetic HFO are very similar (1.8–2.1 wt%) yet when expressed as an H/Fe molar ratio there is a significant difference (factor of ~2). This suggests that OH and H_2O are not primarily coordinating Fe in the HFO structure but rather coordinating the surface cations indiscriminately, in a roughly constant weight fraction because of roughly constant specific areas of reactive surfaces. In other words, it appears that, irrespective of the amounts of Si, C, and As that complex to the surfaces of HFO primary particles, there is always approximately the same number of required OH or H_2O anions per weight of sample to complete the inner sphere coordinations of the exposed or outermost cations. Indeed, a simple calculation that uses typical cation-oxygen bond lengths and the most common coordination geometries allows one to conclude that the amounts of H reported in Table 4 are consistent with ~1 nm diameter primary particles having all their surface cations (Fe^{3+}, As^{5+}, Si^{4+}, C^{4+}) being coordinated on the free surface side by OH^- and OH_2. This is true for both As-HFO and synthetic HFO and the smaller value of the H/Fe ratio for synthetic HFO is interpreted as arising mainly from the As-HFO containing less Fe per primary particle. In other words, the HFO core of an As-HFO primary particle would be smaller than the HFO primary particle of synthetic HFO but the overall primary particles of both As-HFO and synthetic HFO would be of comparable sizes.

Vis-IR diffuse reflectivity

The dry powder vis-IR diffuse reflectivity measurements for the 97R/97Y and V2AR/V2BY couplets are shown in Figure 4, where they are compared to the spectrum for synthetic HFO (pH = 7, [Fe] = 10^{-3} *M*). The diffuse reflectivity in the visible (0.4–0.8 μm) completely determines the hue, value, and chroma color parameters of Munsell (Munsell Soil Color Charts 1994 edition, GretagMacbeth, New Windsor, NY) but not in a simple way that can easily be described quantitatively (Wyszecki and Stiles 1982). Nonetheless, there is a strong correspondence between the hues of our As-HFO samples (Table 1) and the diffuse reflectivity spectra themselves (Fig. 4). The 97R/97Y couplet has the largest Munsell color difference and has the most different spectra, compared to the V2AR/V2BY couplet. V2BY and 97Y have the same hue (10YR) and have strongly overlapping vis-IR spectra in the visible and near-visible regions.

All our As-HFO samples have vis-IR diffuse reflectivity spectra that are very similar to those of all natural Fe oxides and oxyhydroxides (Cornell and Schwertmann 1996; Scheinost et al. 1998). There is no direct indication in the spectra, in the

TABLE 3. XRF results* (in wt% of assumed oxide)

Sample	Fe_2O_3	As_2O_5	SiO_2	Na_2O	CaO	Al_2O_3	MgO	P_2O_5	K_2O	LOI	Total
97R-1	52.1	13.6	21.9	3.6	1.9	1.9	1.6	0.3	0.3	15.9	113.1
97R-2	50.0	4.9	19.1	2.1	1.7	0.3	1.4	0.2	0.3	27.9	107.9
97Y-1	57.8	22.1	12.4	3.7	2.0	0.9	1.2	0.3	0.2	18.4	119.0
97Y-2	56.7	18.8	11.4	1.1	1.8	0.0	1.1	0.3	0.2	22.4	113.8
97Y-3	53.4	20.0	10.7	1.4	1.7	0.0	1.1	0.3	0.2	10.9	99.7
97Y-4	53.2	16.4	10.7	1.7	1.8	0.0	1.1	0.3	0.2	13.9	99.3
97Y-5	56.9	16.2	11.0	1.6	1.8	0.0	1.0	0.3	0.2	12.9	101.9
V2AR	52.6	10.7	17.4	2.7	2.2	1.0	1.0	0.4	0.2	17.9	106.1
V2BY	59.5	19.1	14.9	2.4	2.3	1.1	0.9	0.2	0.2	16.4	117.0
FV1	62.4	13.0	20.3	4.3	2.0	0.5	1.4	0.2	0.2	14.9	119.2
syn-HFO†	85.1	0.0	0.0	1.8	0.0	0.0	0.0	0.0	0.0	13.9	100.8

* All other elements analyzed (Ce, Co, Cr, Cu, Mn, Ni, Pb, Ti, V, Zn) were relatively minor components (less than ~0.1 wt%). Large totals for As-bearing samples are explained in the text.
† pH = 7; [Fe] = 10^{-3} *M*; freeze dried.

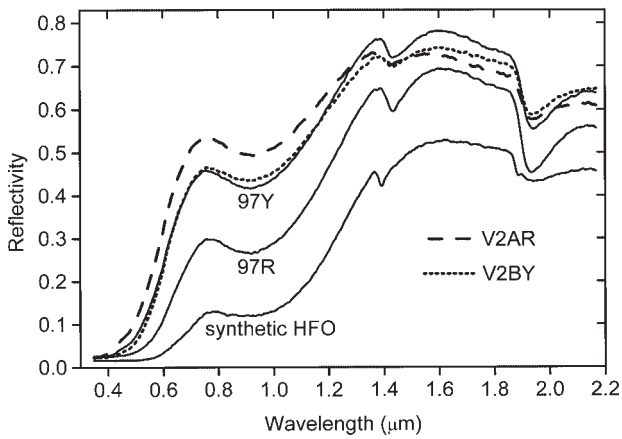

FIGURE 4. Vis-IR diffuse reflectivity for four As-HFO samples and one synthetic HFO sample (pH = 7, [Fe] = 10^{-3}), as indicated.

form of a bending or stretching vibration involving As, that the As-HFO samples contain significant amounts of As. Certain features may be due to the effects of As but these are difficult to identify because there have not been systematic studies of the effects of As on the vis-IR diffuse reflectivity spectra of Fe oxides or oxyhydroxides. The low wavelength region up to ~1 μm is well understood in terms of ligand field transitions of Fe^{3+} in octahedral coordination (Scheinost et al. 1998; Clark et al. 1990). The broad absorption band at ~1.93 μm is due to sorbed and coordinating H_2O whereas the band at ~1.43 μm is due to both H_2O and OH groups (Clark et al. 1990). The spectra therefore offer proof of significant amounts of H_2O, in both As-HFO and synthetic HFO. The presence of significant amounts of OH cannot be ruled out or conclusively established, based on the vis-IR spectra alone.

There are four main features that differentiate the spectra for As-HFO from that for synthetic HFO. First, the overall magnitude of reflectivity is significantly smaller for synthetic HFO, in the entire wavelength region. This is also true when synthetic HFO is compared to natural ferrihydrite (Cornell and Schwertmann 1996) and may be due to an absence of spectroscopically inert (in this region) SiO_2 in the synthetic sample. Second, the main visible-region absorption edge is at ~0.65 μm for synthetic HFO, compared to ~0.58–0.63 μm for As-HFO. The latter absorption edge is known to correlate well with Munsell hue, as is the case here (2.5YR for synthetic HFO, 5YR for 97R, Table 1). We provide an explanation for the latter shift in the next section (Mössbauer section). Third, the H_2O + OH band minimum is at ~1.40 μm for synthetic HFO whereas it is at ~1.43 μm for As-HFO and for natural ferrihydrite (Cornell and Schwertmann 1996). This band is also relatively narrow in synthetic HFO. These facts may be interpreted as evidence for synthetic HFO containing more OH and less H_2O, as is also suggested by its relatively shallow 1.93 μm band. Alternatively or in addition to this, the OH groups in synthetic HFO will coordinate Fe whereas they are likely to coordinate surface complexed As, Si, and C in As-HFO. This may shift the OH stretch frequency by an amount sufficient to explain the observed difference. Finally, the small wavelength edge of the 1.93 μm absorption band is at a smaller wavelength in synthetic HFO than in As-HFO. Given the large width of this band, this may be an artifact of saturation effects.

^{57}Fe Mössbauer spectroscopy

A typical fitted *RT* Mössbauer spectrum (sample 97R) is shown in Figure 5, where it is compared to the *RT* Mössbauer spectrum of a typical synthetic 2-line ferrihydrite sample (pH = 9, [Fe] = 10^{-3} *M*). All the spectra of our As-HFO samples (97R, 97Y, V2AR, V2BY, and FV1), on both velocity ranges used (±11 and ±4 mm/s), are very similar to each other and do not show any detectable amounts of other Fe-bearing phases, such as the common bulk magnetic Fe-oxides (e.g., hematite, goethite) that would show easily detectable sextets (e.g., Kodama et al. 1977). There is a large difference between the *RT* Mössbauer spectra of our As-HFO samples and the *RT* Mössbauer spectra of all known ferrihydrite and ferrihydrite-like materials, including our synthetic 2-line ferrihydrite samples (Thibault 2001), all previously reported synthetic and natural ferrihydrite materials (Cardile 1988; Childs and Johnston 1980; Coey and Readman 1973b; Henmi et al. 1980; Johnston and Lewis 1983; Kauffman and Hazel 1975; Loseva and Murashko 1973; Madsen et al. 1986; Mathalone et al. 1970; Mizota and Maeda 1986; Murad 1988a; Murad 1989; Murad et al. 1988; Murad and Schwertmann 1980; 1988; Rea et al. 1994; Saraswat et al. 1977; Schwertmann and Murad 1988; Van Der Giessen 1967; Vandenberghe et al. 1990; Winnik et al. 1998), ferritin (Brady et al. 1968), and schwertmanite (Murad 1988b). The *LNT* spectra of ferritin are similar to those expected at *RT* (St-Pierre et al. 1986). All the latter materials (irrespective of Si contents) have *RT* Mössbauer spectra that are relatively similar to each other but very different from the *RT* Mössbauer spectra of our As-HFO samples. This difference is clearly seen in the spectra themselves (Fig. 5) and translates into significantly different fitting parameters, on further analysis.

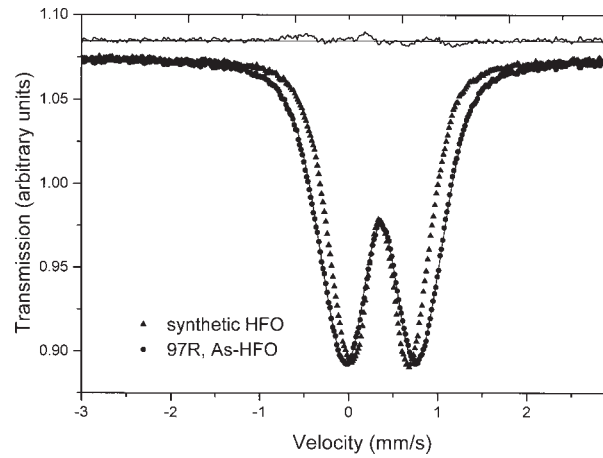

FIGURE 5. *RT* Mössbauer spectrum of As-HFO sample 97R, compared to that of a synthetic HFO sample ([Fe] = 10^{-3} *M*, pH = 9). The fit to the 97R spectrum, that is described in Tables 3 and 4, is shown by a solid line running through the data points and the corresponding residual is shown above the spectra, using the same vertical scale. The two spectra have been rescaled and shifted to facilitate comparison.

Unfortunately, most previous studies have fitted the *RT* spectra of ferrihydrite with Lorentzian doublets, most often using either one or two doublets per spectrum. While this approach provides a quantitative assessment of the spectra, it has many problems such as non-unique solutions arising from parameter tradeoffs and lack of physical meaning of the individual doublets. Rancourt (1994) has shown that this approach is incorrect and has described the problems associated with it. The correct approach in this application is to acknowledge that the physical cause of the absorption lineshape is inhomogeneous broadening arising from a distribution of local environments that gives rise to a QSD (Murad 1989; Vandenberghe et al. 1990). The QSD represents the most crystal chemical information that can be extracted from a spectrum (Rancourt et al. 1994a; Rancourt 1998).

The fit parameters for both *RT* and *LNT* spectra are given in Table 5. Those samples run only at ±11 mm/s (FV1, V2AR, V2BY) were fit with only two QSD components and a CS-QS coupling parameter (δ_1) that was confined to be zero. This gave greater fitting stability and avoided certain artifacts such as extended high-QS QSD tails. Extensive tests showed that, barring such artifacts, the same QSDs were obtained with either two or three (or more) QSD components, within statistical error. Also, freezing δ_1 at zero or letting it adjust had no noticeable affect on the extracted QSD. The spectra collected at *LNT* (samples 97R and 97Y) were fit with two Gaussian QSD components and δ_1 was allowed to have a non-zero value. This was sufficient to give statistically acceptable fits in these cases. Finally, we note that all fits of *RT* spectra, of both synthetic HFO and the As-HFO samples, were significantly improved if we allowed ~5% of intrinsic absorption area asymmetry (A_-/A_+ ~1.05) and that such allowed asymmetry did not change any of the extracted QSDs. Such asymmetry and its physical causes has been described previously in a nanophase oxide (Rancourt et al. 1985) but has not previously been reported in ferrihydrite. It will not be considered further in this article.

Associated calculated parameters are given in Table 6 and are defined as follows: <QS> is the average magnitude (i.e., average absolute value) of the quadrupole splitting (QS), σ_{QSD} is the standard deviation of the QSD, and <CS> is the average CS. These fits and the resulting parameters show that all detectable Fe in our As-HFO samples (and in all ferrihydrite-like

TABLE 6. Calculated Mössbauer parameters

Sample	temperature	<CS>* (mm/s)	<QS> (mm/s)	σ_{QSD} (mm/s)	$<QS>_L$ (mm/s)	Munsell hue (YR)
97R	RT	0.3607	0.913	0.506	0.859	5
97Y	RT	0.3608	0.986	0.499	0.957	10
V2AR	RT	0.3617	0.948	0.449	0.930	7.5
V2BY	RT	0.3604	0.999	0.503	0.962	10
FV1	RT	0.3603	0.892	0.504	0.829	5
syn.-HFO†	RT	0.3470	0.744	0.373	0.717	2.5
97R	LNT	0.3400	0.864	0.444	0.842	5
97Y	LNT	0.3412	0.965	0.496	0.933	10

* With respect to the CS of metallic iron at *RT*, except in LNT measurements where one must add 0.12(1) mm/s (as explained in text). <CS>, <QS>, and σ_{QSD} are from the QSD fits (Table 5) whereas $<QS>_L$ is the average QS obtained from Lorentzian doublet fits, using 2 or 3 Lorentzian doublets arranged symmetrically about similar values of CS.
†pH = 9; [Fe] = 10^{-3} *M*; freeze dried.

TABLE 5. Mössbauer fit parameters*

Sample/ temperature	BG (MC/ch)	Area (kC.mm/s)	δ_0 (mm/s)	δ_1 (%)	p_i (mm/s)	Δ_i (mm/s)	$\sigma_{\Delta i}$	χ^2_{red}
97R	1.0735	0.2716	0.362	–0.0016	5	1.6	1.1	
RT					64	1.00	0.43	
					31	0.597	0.31	1.58
97Y	3.16955	0.7214	0.3703	–0.0096	6	1.9	0.86	
RT					65	1.05	0.393	
					29	0.633	0.255	5.82
V2AR	3.90153	1.2578	0.3617	0.0†	43.7	1.17	0.483	
RT					56.3	0.773	0.344	11.9
V2BY	2.72229	1.0235	0.3604	0.0†	22.5	1.45	0.610	
RT					77.5	0.865	0.389	12.9
FV1	3.13538	0.9350	0.3603	0.0†	16.7	1.42	0.72	
RT					83.3	0.777	0.384	7.92
syn.-HFO‡	0.84436	0.22779	0.3494	–0.0032	14	1.1	0.53	
RT					16	0.453	0.180	
					70	0.76	0.32	1.97
97R	0.13746	41.910	0.3435	–0.0040	32	0.589	0.29	
LNT					68	0.98	0.461	0.61
97Y	0.107084	31.690	0.3478	–0.0069	49	0.735	0.35	
LNT					51	1.18	0.54	0.72

* All parameters are as defined by Rancourt and Ping (1991). In all fits, the Lorentzian full width at half maximum, Γ, was frozen at the known Heisenberg value of 0.097 mm/s. This allows QSDs to be compared directly. Also, only symmetric elemental doublets were used, with $A_-/A_+ = 1.0$, where the latter ratio is the ratio of the spectral area of the low energy Lorentzian line in the elemental doublet to the spectral area of the high energy Lorentzian line in the elemental doublet. Either two or three QSD Gaussian components were used, depending on the number required to obtain a satisfactory fit. BG is the flat background level, in megacounts per channel. Area is the total spectral area. δ_0 and δ_1 are the linear coupling coefficients between CS and QS, as: $CS = \delta_0 + \delta_1(QS)$. p_i is the percent probability of the i-th Gaussian component of the QSD. Δ_i and $\sigma_{\Delta i}$ are the center and sigma-width, respectively, of the i-th Gaussian component of the QSD.
† This parameter was frozen during the fit.
‡ pH = 9; [Fe] = 10^{-3}; freeze dried.

materials) is Fe^{3+}, having parameters consistent with octahedral O coordination, and that there is no detectable tetrahedrally coordinated Fe^{3+} . Tetrahedrally coordinated Fe^{3+} would have a significantly lower CS (Coey 1980; Rancourt et al. 1992) and would give rise to a $^{[4]}Fe^{3+}$ QSD contribution centered at a smaller average QS value and having a smaller width than the $^{[6]}Fe^{3+}$ QSD (Rancourt et al. 1992). Also, the QSs and CSs of $^{[6]}Fe^{3+}$ and $^{[4]}Fe^{3+}$ are expected to have significantly different temperature dependencies (Rancourt et al. 1994b) that would give rise to significant changes in spectral shape on going to *LNT*, for example. This does not occur. The *RT* and *LNT* spectra for a given sample are very similar to each other and have very similar QSD shapes (Tables 5–6). Our conclusion is in contradiction to Cardile's (1988) position that significant amounts of tetrahedral Fe^{3+} may be consistent with the *RT* Mössbauer spectra of ferrihydrite.

The QSDs extracted from the *RT* Mössbauer spectra of all our As-HFO samples and of synthetic 2-line ferrihydrite (pH = 9, [Fe] = 10^{-3} *M*) are compared in Figure 6. As is the case with the spectra themselves, the QSDs of all the As-HFO samples are similar to one another. The most different one from the group (which also has the lowest <QS>, Table 6) is sample FV1. This sample is also the oldest sample that has lost much of its As to a separate As-oxide phase (Fig. 1 and Pichler 1998; Pichler and Veizer 1999). The QSDs show the large systematic differences between the *RT* Mössbauer spectra of our As-HFO samples and As-free ferrihydrite, directly in terms of the local environments of Fe, as expressed in the QSs. The As-HFO samples have significant populations of local environments with large QSs (~1.5 mm/s) whereas As-free ferrihydrite samples do not. The As-HFO QSDs are centered on larger <QS> values, are broader, and have their maxima (i.e., most probable QS values) at ~0.85 mm/s instead of at the typical value of ~0.60 mm/s for As-free ferrihydrite samples.

The QSDs shown in Figure 6 suggest that a large fraction of the Fe (~20%) has local environments that are significantly perturbed by the direct presence of As, via shared coordinating O anions. Given our measured As/Fe ratios (Table 2), this fraction is consistent with a very small primary particle size, such as the sections of double octahedral chains containing only 4–10 Fe^{3+} cations proposed by Waychunas et al. (1996), keeping in mind that one As atom can significantly distort two Fe octahedra in a bidentate arsenate sorption geometry such as the one proposed by Waychunas et al. (1995; 1996). Note that a primary particle containing ~10 Fe atoms and the corresponding numbers of As, Si, and C atoms, consistent with our chemical analyses, would be ~1 nm in diameter, which is comparable to the diameters of primary particles recently seen in synthetic 2-line ferrihydrite by high resolution TEM (Janney et al. 2000). The fact that ~20% of the Fe has local environments that are significantly perturbed by the direct presence of As also means that ~80% of the Fe has local environments similar to those in As-free HFO and allows us to conclude that the As and Fe probably do not mix and are separated in structures consisting of Fe-rich primary particle cores having surface complexed As. This, in turn, suggests that a relatively stable and long lived nucleus of HFO must first be formed before As can complex to it and that Fe-As complexes do not initiate viable nucleus formation during precipitation. The latter scenario is consistent with the Si-As and C-As competitions for surface complexation sites on HFO cores discussed above.

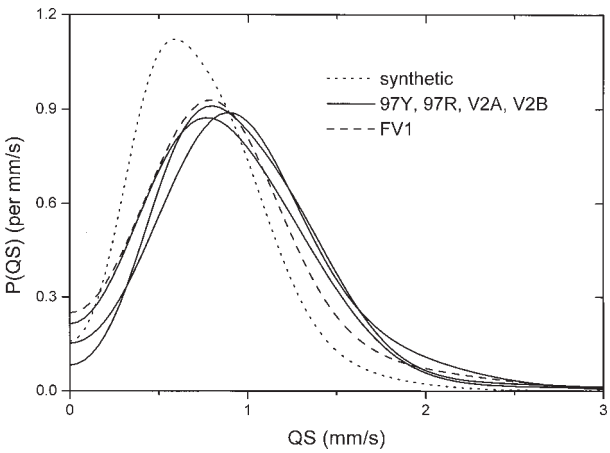

FIGURE 6. The QSDs extracted from the *RT* Mössbauer spectra of As-HFO samples 97Y, 97R, V2AR, V2BY, and FV1, compared to the QSD for a synthetic HFO sample ([Fe] = 10^{-3} *M*, pH = 9).

Although the differences between the QSDs of the relatively pure As-HFO samples (97R, 97Y, V2AR, V2BY; Fig. 6) are small compared to the difference between the QSD of synthetic HFO and the QSDs of the As-HFO samples, they are significant. This is seen on close examination of the corresponding <QS> values (Table 6). The average QS is known to be a robust property of the QSD, that can be estimated from the most common Lorentzian doublet fits if care is taken to avoid CS-QS inter-doublet tradeoffs. Our <QS> values are compared (Table 6) to <QS> values, $\langle QS \rangle_L$, obtained by taking area weighted averages from Lorentzian doublet fits. The latter estimates are seen to systematically underestimate the average QS by ~0.02–0.06 mm/s (0.035 mm/s average underestimate). This arises because the QSD measure is a true average of the QS *magnitude* (since the QSD is a distribution of QS magnitudes) whereas in a Lorentzian doublet approach the effectively negative QS contributions (that have no physical meaning in a paramagnetic doublet context) are not properly taken into account. Nonetheless, $\langle QS \rangle_L$ is a useful quantity because it can be extracted from the most commonly reported Lorentzian doublet fits, thereby allowing important comparisons with published data. As noted above, for example, the $\langle QS \rangle_L$ values for synthetic As-free 2-line ferrihydrite samples occur in the 1σ range 0.66–0.75 mm/s (36 samples) and the $\langle QS \rangle_L$ values for natural As-poor HFO samples occur in the 1σ range 0.69–0.81 mm/s (10 samples) (Thibault 2001). The differences in <QS> (or in $\langle QS \rangle_L$) from one As-HFO sample to another (and with the synthetic HFO sample and literature values) are much larger than the accuracy in determining <QS>. Let us therefore next examine the <QS> values in more detail.

A most striking feature (Table 6) is that <QS> is strongly correlated to the Munsell hue (Table 1 and repeated in Table 6 for convenience). Without exception, there is a near linear relation between the Munsell YR index values (0 is most reddish, 10 is most yellowish) of the As-HFO samples and their <QS> values. A strong correlation is maintained if one adds

the synthetic HFO comparison point, which has the smallest value of Munsell hue YR index. The reddish samples (97R and V2AR) have significantly smaller <QS> values than their yellowish counterparts (97Y and V2BY, respectively), in proportion to their Munsell hue YR index values. This is most probably not an accident and there are good physical reasons to expect such a correlation. The QS is a measure of the degree of local distortion in the octahedral coordination environment of Fe^{3+} and of the lattice contribution to the local electric field gradient and such local distortions and field gradients also determine the molecular orbital energy levels of the Fe^{3+} cation, which in turn determine the main absorption band edge position in the visible, which is the main spectral feature that is associated with the Munsell hue (Scheinost et al. 1998). This correlation therefore establishes that the colors (hues) of our As-HFO samples are mainly determined by the Fe^{3+} cations in their local environments and not by any other chemical constituents (As, Si, C, ...), except indirectly if the latter constituents cause distortions of the Fe^{3+} environments. Since Si and C do not cause significant distortions of the Fe^{3+} environments (as measured by Mössbauer QSs) and since As content is strongly correlated to Munsell hue (Tables 1–3), As must be the main cause of the increased QSs and associated changes in the Fe^{3+} local environments. There can be no doubt that As is in close coordination proximity to Fe. The quite striking yellowish hues of our As-HFO samples are caused by As, which, by complexation, distorts the local environments of a large fraction of the $^{[6]}Fe^{3+}$ cations thereby changing their electronic orbital structures in such a way as to cause a significant shift of the main visible absorption band edge. It is likely that this mechanism also causes the yellowish colors that are correlated to As contents in Si-poor As-rich As-HFO formed in acid mine drainage environments (Leblanc et al. 1996), in further support of the conclusion that Si does not play a significant role in determining the hue. We also note that the small amounts of smectite-illite that are detected by pXRD in the reddish samples (V2AR and 97R) are not expected to contribute significant features to the measured QSDs. Indeed, the known $\langle QS \rangle_L$ of the main $^{[6]}Fe^{3+}$-bearing smectite, nontronite, is 0.44(4) mm/s (average for 22 samples, unpublished), a value that precludes any interference with the main QSD feature at ~1.5 mm/s that we attribute to As complexation.

Finally, our <QS> values for As-HFO samples measured at *RT* (Table 6) can be compared to two relevant measurements. First, Rea et al. (1994) measured the $\langle QS \rangle_L$ (calculated from a Lorentzian doublet fit) of a synthetic ferrihydrite sample in which the most labile surface sites were isotopically enriched in ^{57}Fe and obtained 0.87 mm/s (their sample MF6). This value is significantly larger than typical values for ferrihydrite materials and approaches or surpasses our values for As-HFO samples. For example, it surpasses the $\langle QS \rangle_L$ value of 0.829 mm/s for sample FV1 which has presumably lost much of its As to a more stable As-oxide phase. From this comparison we conclude that both the most labile sites in As-free samples and As-perturbed sites in As-HFO have larger QSs (and local distortions) than interior sites but that the perturbing effect of As is much larger than that of the surface. Second, Rea et al. (1994) also measured the $\langle QS \rangle_L$ of a synthetic sample that was first surface enriched in ^{57}Fe and then sorbed with As and obtained 0.78 mm/s. The latter value is in the range of As-poor natural HFO samples (0.69–0.81 mm/s) and is close to the 1σ range of As-free synthetic HFO samples (0.66–0.75 mm/s). It is also lower than their value for As-free labile sites and this was interpreted to mean that As decreased the distortion of the surface sites. The latter result and interpretation is in conflict with our results that demonstrate a large <QS> enhancement arising from As. This may be due to a fundamental structural difference between samples sorbed with As after synthesis vs. samples that are the result of rapid coprecipitation or it may be due to transformations that occurred under the particular isotopic exchange and sorption conditions that were used (Rea et al. 1994).

SQUID Magnetometry

Magnetometry is a powerful materials characterization tool and is particularly useful with iron oxides and oxyhydroxides because they exhibit various magnetic behaviors, such as magnetic ordering, spin-flop transitions, electron localization, mixed valences, superparamagnetism, superferromagnetism, and incomplete antiferromagnetic sublattice cancellation, that are very sensitive to their crystal chemical and microstructural features (e.g., Dang et al. 1998; Dunlop and Özdemir 1997). Magnetism has often been used as a sensitive characterization of HFO-like materials, including synthetic and natural ferrihydrite samples, a commercial ferrihydrite-like catalysis material (NANOCAT, manufactured by Mach I, Inc.), and various types of ferritin, using both variable field and temperature Mössbauer spectroscopy (Bauminger and Nowik 1989; Cianchi et al. 1994; 1992; Coey and Readman 1973a; Hawkins et al. 1994; Madsen et al. 1986; Murad et al. 1988; Pankhurst and Pollard 1992; Pollard et al. 1992; Quin et al. 1988; St-Pierre et al. 1996; 1989; Zhao et al. 1996) and classic magnetometry measurements (Allen et al. 1998; Coey and Readman 1973b; Gider et al. 1995; Ibrahim et al. 1994; 1995; Lear 1987; Van Der Giessen 1967).

The zero-field quench FW susceptibilities (M/H) for our As-HFO samples (excluding FV1 which has significant amounts of crystalline phase impurities) and for three synthetic HFO samples are shown in Figures 7 and 8, respectively, where they are compared to the theoretical curves for paramagnets containing the same numbers of ferric cations per gram as synthetic HFO and natural Si-bearing As-HFO. The theoretical susceptibility of a paramagnet is given by the well known Curie law, in which we assume orbital quenching (L = 0) and a total electronic spin S = 5/2 for ferric iron. The only required sample-dependent parameter is the number of paramagnetic cations (Fe^{3+}) per gram of sample. All other ionic and molecular species (OH^-, O^{2-}, As^{3+}, As^{5+}, Si^{4+}, Na^+, Ca^{2+}, Al^{3+}, P^{5+}, K^+, Mg^{2+}, C^{4+}, and H_2O) are strictly diamagnetic. Assuming any of the most common stoichiometric formulas (such as $Fe_5HO_8{\cdot}4H_2O$, $5Fe_2O_3{\cdot}9H_2O$, or $Fe_2O_3{\cdot}2FeOOH{\cdot}2.6H_2O$; see Jambor and Dutrizac 1998) for ferrihydrite leads to the same number of Fe per unit mass: $N_g = 6.27 \times 10^{21}$ Fe/g. Using As/Fe = 0.15 and Si/Fe = 0.3 as representative numbers (Tables 2 and 3 and associated discussions) and ignoring C (Table 4), we then assume a reasonable formula for As-HFO of $5Fe_2O_3{\cdot}9H_2O{\cdot}3SiO_2{\cdot}0.75As_2O_5$ to obtain $N_g = 4.585 \times 10^{21}$ Fe/

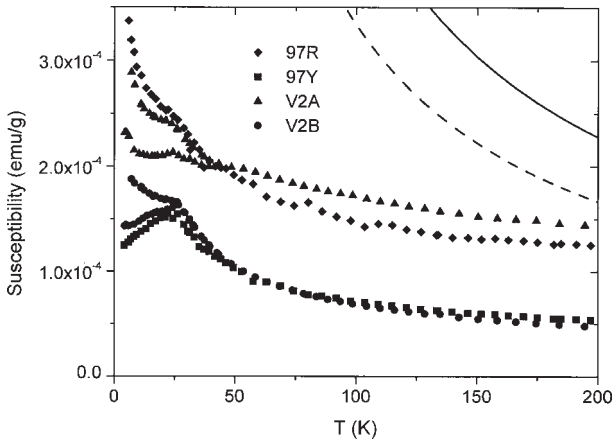

FIGURE 7. Low-field magnetic susceptibility (M/H) vs. temperature for As-HFO samples 97R, 97Y, V2AR, and V2BY (as indicated), compared to the theoretical susceptibilities corresponding to the pure paramagnetism of a representative synthetic HFO (solid line) and to the pure paramagnetism of a representative As-HFO (dashed line). Both FW and FC data are shown for samples V2AR and V2BY. The FW and FC data merge at ~25 K for sample V2BY and at ~45 K for sample V2AR. The FC values are always larger than or equal to the FW values. A superparamagnetism to superferromagnetism transition occurs at 25 K in these samples.

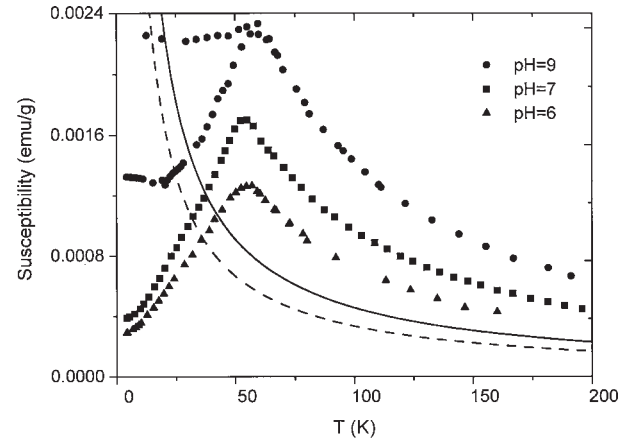

FIGURE 8. Low-field magnetic susceptibility vs. temperature for synthetic HFO samples ([Fe] = 10^{-3} *M*; pH = 6, 7, 9, as indicated), compared to the theoretical susceptibilities corresponding to the pure paramagnetism of a representative synthetic HFO (solid line) and to the pure paramagnetism of a representative As-HFO (dashed line). Only FW data is shown for pH = 6 and 7, whereas both FW and FC data is shown for pH = 9. The superparamagnetism to superferromagnetism transition occurs at 55–59 K in these samples.

g. The resulting theoretical susceptibilities are shown as solid and dashed curves, respectively, in Figures 7 and 8. These curves give a reference point corresponding to a total absence of inter-moment interactions, such as those that cause superparamagnetism, superferromagnetism, antiferromagnetism and ferrimagnetism, and they allow a clearer comparison of HFO and As-HFO.

Superparamagnetism is the phenomenon whereby the supermoments on individual primary particles, that arise from intra-particle inter-atomic magnetic exchange interactions at temperatures sufficiently below the intrinsic magnetic ordering temperature (Néel or Curie point) of the material, have random fluctuations in orientation due to thermal excitation, much as individual atomic moments have thermal fluctuations in the usual paramagnetic state (Dormann et al. 1997). Superferromagnetism is the phenomenon in which the supermoments of superparamagnetic particles order magnetically, under the influence of inter-particle magnetic interactions. The latter interactions can be purely dipolar in nature or can have an exchange component from inter-particle bridges. The unusual magnetism of ferrihydrite and HFO samples has been interpreted in terms of these phenomena (Bauminger and Nowik 1989; Cianchi et al. 1994; 1992; Hawkins et al. 1994; Madsen et al. 1986; Murad et al. 1988; Pankhurst and Pollard 1992; Pollard et al. 1992; Quin et al. 1988; St-Pierre et al. 1996; 1989; Allen et al. 1998; Coey and Readman 1973a; 1973b; Gider et al. 1995; Ibrahim et al. 1994; 1995; Van Der Giessen 1967; Zhao et al. 1996), where the primary (~1–5 nm) particles have a transition from paramagnetism to superparamagnetism, as temperature is decreased, at or near the intrinsic magnetic ordering temperature of the material (ferrihydrite), $T_{P/SP}$, followed by a transition from superparamagnetism to superferromagnetism at some lower temperature, $T_{SP/SF}$. The blocking temperature, T_B, is defined as the temperature at which, on decreasing the temperature, the superparamagnetic fluctuations are observed to effectively stop, in a given measurement. Clearly, T_B is not a uniquely defined property of the sample in that it depends on the measurement time of the probe being used. The relation between T_B and $T_{SP/SF}$ and relevant concepts have been discussed by Rancourt and Daniels (1984). Because of the relation to various technological applications, the area of small particle magnetism is presently one of intense fundamental research, with significant advances in understanding being made in both superparamagnetism (e.g., Coffey et al. 1998) and superferromagnetism (e.g., García-Otero et al. 2000; Nowak et al. 2000).

The magnetic behaviors of our As-HFO and synthetic HFO samples can be understood in terms of the above concepts and the usual ferrimagnetism that is common in iron oxide particles (e.g., Dang et al. 1998). The main features and their interpretation are described below. We find that the magnetic behaviors of HFO and As-HFO are dramatically different, far more than the mass dilution of paramagnetic cations caused by the adsorbed arsenate and incorporated or adsorbed Si or C would suggest. The main differences are related to significant differences in structure and microstructure, as discussed below.

Superparamagnetic/superferromagnetic transitions are seen in all the samples, where $T_{SP/SF}$ is estimated as the temperature at which a sharp cusp (or maximum) occurs in the FW curve. The latter temperature of the maximum in the FW curve is also usually close to the temperature at which temperature hysteresis sets in. That is, the temperature at which the FW and FC curves depart significantly on cooling. In all our synthetic HFO samples (pH = 6, 7, 9; [Fe] = 10^{-3} *M*), we find $T_{SP/SF}$ = 55–59 K (Fig. 8) whereas all the As-HFO samples (except FV1 which

has significant amounts of crystalline phase impurities; Table 1, Fig. 1) have clear signs of a transition at $T_{SP/SF}$ = 25 ± 2 K (Fig. 7). In the yellowish (more As-rich, 97Y and V2BY) samples a true FW maximum occurs at 25 K whereas in the reddish (97R and V2AR) samples a weaker peak is seen at 25 K to be superposed on a paramagnetic or superparamagnetic Curie-like contribution (Fig. 7). This suggests that the reddish samples may have inhomogeneous magnetic responses with some of the material in a given reddish sample having a superferromagnetic ordering temperature of 25 K and the other fraction of the material having lower superferromagnetic ordering temperatures, below 4.2 K since another FW peak is not seen. The Curie-like contributions in the FW and FC curves of the reddish samples may be superparamagnetic signals from fractions within the samples that have low superferromagnetic ordering temperatures. Part of the Curie-like contributions may also arise from the ordinary paramagnetism of exchange isolated or loose Fe^{3+} moments.

$T_{SP/SF}$ is a consequence of several factors such as: supermoment magnitude, μ, mean inter-particle distance, *d*, strength of inter-particle magnetic bridging, via superexchange shared oxygen bonds, etc. For example, for pure dipolar interparticle interactions and a given primary particle spatial configuration, we have $T_{SP/SF} \propto \mu^2/d^3$. If primary particle packing is optimum and the supermoment is proportional to the primary particle volume, then $T_{SP/SF} \propto r^3$, where r is the primary particle radius. This suggests that As-HFO material having $T_{SP/SF}$ ~25 K has primary particles that are simply smaller than the synthetic HFO primary particles, by ~25%. As-HFO material having $T_{SP/SF}$ approximately < 4 K would have primary particles that are much smaller than the primary particles in synthetic HFO. Alternatively, if the inter-particle separation is the same for As-HFO and synthetic HFO, one can interpret the lower value of $T_{SP/SF}$ = 25 K for As-HFO as meaning that the material having this lower value of $T_{SP/SF}$ has supermoments that are ~30% smaller than the supermoments of synthetic HFO. Similarly, $T_{SP/SF}$ approximately < 4 K values would imply a much smaller supermoment magnitude. On the other hand, inter-particle exchange interaction bridging may play a role and sorbed OH/OH_2 coordinated complexes of As (and Si and C, to different extents) may poison such bridging in the As-HFO agglomerations of primary particles, thereby causing the observed reduced values of $T_{SP/SF}$.

The susceptibilities themselves have typical magnitudes that are much greater for our synthetic HFO samples than for our As-HFO samples. There is approximately a factor of 10 difference in the susceptibility magnitudes (Figs. 7–8), with the HFO susceptibilities being significantly larger than expected paramagnetic HFO values (Fig. 8) and the As-HFO susceptibilities being significantly smaller than expected paramagnetic As-HFO values (Fig. 7). This unusual situation can be understood in terms of certain features of small magnetic particles, as follows. The ratio of susceptibilities for ordinary paramagnetic (Curie law) behavior and for superparamagnetic (Langevin-type) behavior can be expressed as the ratio of the usual Curie constant, C_J, for cations of spin *J*, and the effective Curie constant, C_L, for Langevin-type superparamagnetism. Assuming one supermoment per primary particle, it can be shown that

$$C_L/C_J = (m^2/n)\,[J/(J+1)] \quad (1)$$

where *n* is the number of moment-bearing cations in a primary particle and m is the number of atomic moments per supermoment. One atomic (or cationic) moment has magnitude $\mu_a = gJ\mu_B$ where *g* is the Landé *g*-factor and μ_B is the Bohr magneton. In all cases considered here J = S = 5/2 for Fe^{3+} but the factor m^2/n in Equation 1 can be: (a) comparable to 1, if $m \sim n^{1/2}$ as expected for random vacancies in a two-sublattice antiferromagnet (see Dormann et al. 1997); (b) larger than 1, if $m > n^{1/2}$ as occurs with ferromagnetic particles where $m^2/n \propto r^3$; or (c) smaller than 1, if $m < n^{1/2}$ as occurs when, for example, a sufficiently small antiferromagnetic particle has mostly paired opposing nearest neighbor moments. Clearly, in small particle systems all situations are possible. Our results suggest that the synthetic HFO samples and the As-HFO samples differ significantly in their mechanisms for creating a resulting net supermoment per primary particle. Synthetic HFO must have $m^2/n > 1$ whereas As-HFO must have $m^2/n < 1$. There is also a systematic difference between the susceptibility magnitudes of the reddish (97R and V2AR) and yellowish (97Y and V2BY) samples (Fig. 7) that implies that the yellowish (As-rich) samples have values of m^2/n that are smaller than those of the reddish samples. Differences in m^2/n can arise from purely geometric effects related to primary particle size and shape but can also involve differences in intra-particle surface moment coupling due to the presence or absence of sorbed As. The above Mössbauer results show that a significant fraction of the Fe in As-HFO has significantly distorted local environments, relative to those in HFO. Such distortions in Fe-O bond lengths and bond angles are known to significantly affect inter-atomic magnetic superexchange bond strengths. This is consistent with the more As-rich (yellowish) samples having the smallest values of m^2/n, the order being synthetic-HFO > reddish-As-HFO > yellowish-As-HFO.

On examination of the magnetometry results for the As-HFO samples (Fig. 7), one notes that the susceptibilities for samples 97Y and V2BY are almost identical, whereas they are step-wise different from the susceptibilities for samples 97R and V2AR, which are very similar to each other. This grouping correlates with the colors of the samples (Table 1), their chemical compositions (Tables 2–4), and their Mössbauer parameters (Tables 5–6). The measurements taken together, and the magnetometry results in particular, suggest a bimodal population of As-HFO deposits consisting of materials that are either reddish or yellowish in character, where As-HFO materials of intermediate character are avoided. In other words, the observed banding (Picher 1998; Pichler and Veizer 1999) seems to be well defined.

Further discussion and conclusion

We find the natural As-HFO to be very similar to those synthetic As-HFO materials formed by coprecipitation, as opposed to sorption of As after HFO synthesis, and to be significantly different from all As-free related materials, including all known synthetic and natural HFO materials and ferrihydrite samples. As is the case for 2-line ferrihydrite and most HFO materials, a low degree of crystallinity (including both structural disorder

and small particle size effects) does not allow a structural determination but the data does permit many features of the microstructures and local structures to be described. All the data either support or are consistent with As-HFO being a nanophase material in which there is intimate molecular-scale association of tetrahedrally coordinated arsenate with Fe in a typical oxyhydroxide framework of octahedrally coordinated Fe^{3+} and in which there is significant inter-particle agglomeration (or bridging or consolidation). The As seems to prevent particle growth and cause smaller HFO primary particles (or cores) to be formed, even compared to the effects of surface complexed Si and C. It also causes more structural disorder, in the form of significantly distorted octahedral environments of Fe. The latter distortions that are caused by As, since Si and C have much weaker effects, perturb the $^{[6]}Fe^{3+}$ electronic orbitals and their energy levels which, in turn, results in both larger QSs and shifted visible absorption band edges, thereby causing the observed strong correlation between Munsell hue and Mössbauer parameters. In addition, the QS of Fe^{3+} is expected to have a large lattice (i.e., ionic point charge distribution) contribution that will also be affected by the presence of nearby As^{5+}. The As also appears to be relatively strongly complexed to the HFO core, compared to Si or C, such that it more effectively retards evolution toward more stable crystalline phases that, initially, are smectite-illite mixtures and claudetite.

Overall, the observed effects that can be unambiguously attributed to As, as opposed to other sorbed or surface complexed species such as Si and C, include: (1) modifications of the pXRD pattern, relative to the 2-line patterns of As-free or As-poor HFO materials, indicating the intimate association of Fe and As; (2) relatively large QS values in the *RT* Mössbauer spectra that correspond to significantly distorted octahedral Fe^{3+} environments, again attesting to an atomic scale association of Fe and As; (3) a shift toward smaller wavelengths of the main absorption band edge in the visible and a corresponding increase of the Munsell hue YR index that occur in proportion to the amount of complexed As; and (4) stabilization of the As-HFO structure with respect to kinetic transformation toward more crystalline phases. In addition, it seems likely, as indicated by the magnetometry results, that As is responsible for producing particularly small HFO primary particles or cores (with $m^2/n < 1$) and that the smaller of these (more As, yellowish samples) have mainly even numbers of magnetic moment bearing Fe^{3+} cations whereas the larger ones (less As, reddish samples) have larger probabilities of containing odd numbers of Fe^{3+} cations. The latter interpretation would explain both the larger paramagnetic Curie-type contributions (e.g., Rancourt et al. 1986) and the larger susceptibility magnitudes (i.e., larger m^2/n values from larger supermoments arising from unpaired moments) of the relatively As-poor (reddish) As-HFO samples. Finally, the chemical compositions indicate another interesting effect arising from the presence of As: There seems to be an avoidance interaction or competition between the complexation of As and the complexation of Si and C onto HFO binding sites, giving rise to a strong anticorrelation between As and Si or C.

Complexed arsenate seems to stabilize the structure and retard the transformation to more stable As and Fe-bearing phases, as suggested by the increased thermal stability of the synthetic As-HFO materials. This apparent correlation between disorder and metastability is not contradictory; if the reaction free energy to coprecipitate As-HFO is large then the kinetics are likely to be rapid and relatively disordered structures can result. More work is needed to characterize the evolution of the natural As-HFO materials toward the more stable phases, including the initial stages that involve the distinct yellowish (samples 97Y and V2BY) and reddish (samples 97R and V2AR) layers that we have described. The type of As–Si/C avoidance interaction described above may drive the banding that occurs in the As-HFO deposits, via post-deposition surface diffusion across compact agglomerations of primary particles. Alternatively, the banding may be a record of variations in hydrothermal fluid or seawater characteristics. More work is also needed to more fully characterize the As-HFO materials themselves. High resolution TEM, along the lines of the recent work on synthetic HFO by Janney et al. (2000), would be particularly welcome in the latter area, as would the use of ab initio quantum mechanical calculations of sorption and complexation, along the lines of the recent work by Randall et al. (1999).

ACKNOWLEDGMENTS

Financial support from the Natural Sciences and Engineering Research Council of Canada is gratefully acknowledged. Thomas Pichler acknowledges support in the form of Geological Society of America student research grants. We thank Nathalie Roux, Milena Kusnir, and Gabriella Giustiniano for performing several of the syntheses and characterizations related to the synthetic ferrihydrite reference material and co-investigator Denis Mavrocordatos for allowing us to use unpublished data from the later study. The TEM/EDS measurements were performed at the University of Guelph, in T.J. Beveridge's laboratory. This work was supported in part by NASA's Cosmochemistry Program under RTOP 344-31-20-24 (R.V.M.). We thank Ron Hartree for his help in establishing the required XRF calibrations and procedures. We thank Mei-Zhen Dang, Wendy Abdi, and Gilles St-Jean for their work in establishing the required GC calibrations and procedures. We have benefitted from the often very detailed and extensive comments of four anonymous reviewers whom we thank.

REFERENCES CITED

Aggett, J. and O'Brien, G.A. (1985) Detailed model for the mobility of arsenic in lacustrine sediments based on measurements in Lake Ohakuri. Environmental Science and Technology, 19, 231–244.

Allen, P.D., St-Pierre, T.G., and Street, R. (1998) Magnetic interactions in native horse spleen ferritin below the superparamagnetic blocking temperature. Journal of the Magnetism and Magnetic Materials, 177–181, 1459–1460.

Bauminger, E.R. and Nowik, I. (1989) Magnetism in plant and mammalian ferritin. Hyperfine Interactions, 50, 484–498.

Belzile, N. (1988) The fate of arsenic in sediments of the Laurentian Trough. Geochimica et Cosmochimica Acta, 52, 2293–2302.

Belzile, N. and Tessier, A. (1990) Interactions between arsenic and iron oxyhydroxides in lacustrine sediments. Geochimica and Cosmochimica Acta, 54, 103–109.

Bowell, R.J. (1994) Sorption of arsenic by iron oxides and oxyhydroxides in soils. Applied Geochemistry, 9, 279–286.

Boyd, T. and Scott, S.D. (1999) Two-XRD-line ferrihydrite and Fe-Si-Mn oxyhydroxide mineralization from Franklin Seamount, Western Woodlark Basin, Papua New Guinea. Canadian Mineralogist, 37, 973–990.

Brady, G.W., Kurkjian, C.R., Lyden, E.F.X., Robin, M.B., Saltman, P., Spiro, T., and Terzis, A. (1968) The structure of an iron core analog of Ferritin. Biochemistry, 7, 2185–2192.

Buckingham, W.F. and Sommer, S.E. (1983) Mineralogical characterization of rock surfaces formed by hydrothermal alteration and weathering—Application to remote sensing. Economic Geology, 78, 664–674.

Cardile, C.H. (1988) Tetrahedral Fe^{3+} in ferrihydrite: ^{57}Fe Mössbauer spectroscopy evidence. Clays and Clay Minerals, 36, 537–539.

Childs, C.W. (1992) Ferrihydrite: A review of structure, properties, and occurrence in relation to soils. Zeitschrift für Pflanzenernahrung und bodenkunde, 155, 441–448.

Childs, C.W. and Johnston, J.H. (1980) Mossbauer spectra of proto-ferrihydrite at 77k and 295k, and a reappraisal of the possible presence of akaganeite in New Zealand soils. Australian Journal of Soil Research, 18, 245–250.

Cianchi, L., Gulisano, F., and Spina, G. (1994) Isotropic relaxation of the hyperfine field and intercluster interactions in ferrihydrite. Journal of Physics—Condensed Matter, 6, 2269–2275.
Cianchi, L., Mancini, M., Spina, G., and Tang, H. (1992) Mossbauer spectra of ferrihydrite: superferromagnetic interactions and anisotropy local energy. Journal of Physics—Condensed Matter, 4, 2073–2077.
Clark, R.N., King, T.V.V., Klejwa, M., and Swayze, G.A. (1990) High spectral resolution reflectance spectroscopy of minerals. Journal of Geophysical Research, 95, 12653–12680.
Coey, J.M.D. (1980) Clay minerals and their transformations studied with nuclear techniques: The contribution of Mössbauer spectroscopy. Atomic Energy Review, 18, 73–124.
Coey, J.M.D. and Readman, P.W. (1973a) New spin structure in an amorphous ferric gel. Nature, 246, 476–478.
———(1973b) Characterization and magnetic properties of natural ferric gel. Earth and Planetary Science Letters, 21, 45–51.
Coffey, W.T., Crothers, D.S.F., Dormann, J.L., Kalmykov, Yu.P., Kennedy, E.C., and Wernsdorfer, W. (1998) Thermally activated relaxtion time of a single domain ferromagnetic particle subjected to a uniform field at an oblique angle to the easy axis: Comparison with experimental observations. Physical Review Letters, 80, 5655–5658.
Cornell, R.M. and Schwertmann, U. (1996) The Iron Oxides (VCH, Weinheim) pp. 573.
Cullen, W.R. and Reimer, K.J. (1989) Arsenic speciation in the environment. Chemical Reviews, 89, 713–764.
Dang, M.-Z., Rancourt, D.G., Dutrizac, J.E., Lamarche, G., and Provencher, R. (1998) Interplay of surface conditions, particle size, stoichiometry, cell parameters, and magnetism in synthetic hematite-like materials. Hyperfine Interactions, 117, 271–319.
De Carlo, E.H. and Thomas, D.M. (1985) Removal of arsenic from geothermal fluids by adsorptive bubble flotation with colloidal ferric hydroxide. Environmental Science and Technology, 19, 538–544.
Deer, W.A., Howie, R.A., and Zussman, J. (1966) An introduction to the rock forming minerals, 528 p. Longman, London, U.K.
Dormann, J.L., Fiorani, D., and Tronc, E. (1997) Magnetic relaxation in fine-particle systems. In I. Prigogine and S.A. Rice, Eds., Advances in Chemical Physics, vol. XCVIII, p. 283–494. Wiley, New York.
Driehaus, W., Jekel, M., and Hildebrandt, U. (1998) Granular ferric hydroxide – a new adsorbent for the removal of arsenic from natural water. Journal Water SRT – Aqua, 47, 30–35.
Dunlop, D.J. and Özdemir, Ö. (1997) Rock magnetism: Fundamentals and frontiers, p. 573. Cambridge University Press, U.K.
Edenborn, H.M., Belzile, N., Mucci, A., Lebel, J., and Silverberg, N. (1986) Observations on the diagenetic behavior of arsenic in a deep coastal sediment. Biogeochemistry, 2, 359–376.
Fortin, D., Ferris, F.G., and Scott, S.D. (1998) Formation of Fe-silicates and Fe-oxides on bacterial surfaces in samples collected near hydrothermal vents on the southern explorer ridge in the southern pacific ocean. American Mineralogist, 83, 1399–1408.
Fuller, C.C., Davis, J.A., and Waychunas, G.A. (1993) Surface chemistry of ferrihydrite: Part 2. Kinetics of arsenate adsorption and coprecipitation. Geochimica and Cosmochimica Acta, 57, 2271–2282.
Garcia-Otero, J., Porto, M., Rivas, J., and Bunde, A. (2000) Influence of dipolar interaction on magnetic properties of ultrafine ferromagnetic particles. Physical Review Letters, 84, 167–170.
Gider, S., Awschalom, D.D., Douglas, T., Mann, S., and Chaparala, M. (1995) Classical and quantum magnetic phenomena in natural and artificial ferritin proteins. Science, 268, 77–80.
Glasauer, S.M., Hug, P., Weidler, P.G., and Gehring, A.U. (2000) Inhibition of sintering by Si during the conversion of Si-rich ferrihydrite to hematite. Clays and Clay Minerals, 48, 51–56.
Hawkins, C., Williams, J.M., Hudson, A.J., Andrews, S.C., and Treffry, A. (1994) Mossbauer studies of the ultrafine antiferromagnetic cores of ferritin. Hyperfine Interactions, 91, 827–833.
Henmi, T., Wells, N., Childs, C.W., and Parfitt, R.L. (1980) Poorly ordered iron-rich precipitates from springs and streams on andesitic volcanoes. Geochimica et Cosmochimica Acta, 44, 365–372.
Hering, J.G., Chen, P.-Y., Wilkie, J.A., Elimelech, M., and Liang, S. (1996) Arsenic removal by ferric chloride. Journal American Water Works Association, 88, 155–167.
Hering, J.G., Chen, P.-Y., Wilkie, J.A., and Elimelech, M. (1997) Arsenic removal from drinking water during coagulation. Journal of Environmental Engineering, August, 800–807.
Hess, R.E. and Blanchar, R.W. (1976) Arsenic stability in contaminated soils. Soil Science Society of America Journal, 40, 847–852.
Ibrahim, M.M., Darwish, S., and Seehra, M.S. (1995) Nonlinear temperature variation of magnetic viscosity in nanoscale FeOOH particles. Physical Review B, 51, 2955–2959.
Ibrahim, M.M., Edwards, G., Seehra, M.S., Ganguly, B., and Huffman, G.P. (1994) Magnetism and spin dynamics of nanoscale FeOOH particles. Journal of Applied Physics, 75, 5873–5875.
Jambor, J.L. and Dutrizac, J.E. (1998) Occurrence and constitution of natural and synthetic ferrihydrite, a widespread iron oxyhydroxide. Chemical Reviews, 98, 2549–2585.
Janney, D.E., Cowley, J.M., and Buseck, P.R. (2000) Transmission electron microscopy of synthetic 2- and 6-line ferrihydrite. Clays and Clay Minerals, 48, 111–119.
Johnston, J.H. and Lewis, D.G. (1983) A detailed study of the transformation of ferrihydrite to hematite in an aqueous medium at 92 °C. Geochimica et Cosmochimica Acta, 47, 1823–1831.
Juniper, S.K. and Fouquet, Y. (1988) Filamentous iron-silica deposits from modern and ancient hydrothermal sites. Canadian Mineralogist, 26, 859–869.
Kauffman, K. and Hazel, F. (1975) Mossbauer spectroscopy of aged ferric oxide gels. Journal of Colloid and Interface Science, 51, 422–426.
Kodama, H., McKeague, J.A., Tremblay, R.J., Gosselin, J.R., and Townsend, M.G. (1977) Characterization of iron oxide compounds in soils by Mossbauer and other methods. Canadian Journal of Earth Sciences, 14, 1–15.
Lamarche, G. (1989) Simple top-loading cryostat insert for a SQUID magnetometer. Review of Scientific Instruments, 60, 943–945.
Lear, P.R. (1987) The role of iron in nontronite and ferrihydrite. Ph.D. thesis. University of Illinois at Urbana-Champaign. p. 119.
Leblanc, M., Achard, B., Ben Othman, D., Luck, J.M., Bertrand-Sarfati, J., and Personné, J.Ch. (1996) Accumulation of arsenic from acidic mine waters by ferruginous bacterial accretions (stromatolites). Applied Geochemistry, 11, 541–554.
Lee, B.-G., Griscom, S.B., Lee, J.-S., Choi, H.J., Koh, C.-H., Luoma, S.N., and Fisher, N.S. (2000) Influences of dietary uptake and reactive sulfides on metal bioavailability from aquatic sediments. Science, 287, 282–284.
Loseva, G.V. and Murashko, N.V. (1973) Use of Mossbauer spectroscopy to investigate formation of hematite from amorphous iron hydroxide. Neorganicheskie Materialy, 9, 1301–1302.
Madsen, M.B., Morup, S., and Koch, C.J.W. (1986) Magnetic properties of ferrihydrite. Hyperfine Interactions, 27, 329–332.
Maher, W.A. (1984) Arsenic in marine organisms—A minireview. Biological Trace Element Research, 6, 159–164.
Maher, W. and Butler, E. (1988) Arsenic in the marine environment. Applied Organometallic Chemistry, 2, 191–214.
Manceau, A. (1995) The mechanism of anion adsorption on iron oxides: Evidence for the bonding of arsenate tetrahedra on free $Fe(O,OH)_6$ edges. Geochimica and Cosmochimica Acta, 59, 3647–3653.
Mathalone, Z., Ron, M., and Biran, A. (1970) Magnetic ordering in iron gel. Solid State Communications, 8, 333–336.
Mizota, M. and Maeda, Y. (1986) Magnetite in the radular teeth of chitons. Hyperfine Interactions, 29, 1423–1426.
Mok, W.M. and Wai, C.M. (1994) In J.O. Nriagu, Ed., Arsenic in the Environment, Part I: Cycling and Characterization, p. 99–118. Wiley, New York.
Murad, E. (1988a) Properties and behavior of iron oxides as determined by Mossbauer spectroscopy. In J.W. Stucki, B.A. Goodman, and U. Schwertmann, Eds., Iron in soils and clay minerals, vol. 217, p. 309–350. Proceedings of the NATO ASI, Bad Windsheim (Germany), Kluwer Academic Publishers, AA Dordrecht, the Netherlands.
———(1988b) The Mossbauer spectrum of "well" crystallized ferrihydrite. Journal of Magnetism and Magnetic Materials, 74, 153–157.
———(1989) Poorly crystalline minerals and complex mineral assemblages. Hyperfine Interactions, 47, 33–53.
Murad, E. and Schwertmann, U. (1980) The Mossbauer spectrum of ferrihydrite and its relations to those of other iron oxides. American Mineralogist, 65, 1044–1049.
Murad, E. and Schwertmann, U. (1988) The characterization of poorly crystalline Si-containing natural iron oxides by Mossbauer spectroscopy. Hyperfine Interactions, 41, 835–838.
Murad, E., Bowen, L.H., Long, G.L., and Quin, T.G. (1988) The influence of crystallinity on magnetic ordering in natural ferrihydrites. Clay Minerals, 23, 161–173.
Nowak, U., Chantrell, R.W., and Kennedy, E.C. (2000) Monte Carlo simulation with time step quantification in terms of Langevin dynamics. Physical Review Letters, 84, 163–166.
Pankhurst, Q.A. and Pollard, R.J. (1992) Structural and magnetic properties of ferrihydrite. Clays and Clay Minerals, 40, 268–272.
Parfitt, R.L. (1978) Anion adsorption by soils and soil materials. In A.G. Norman, Ed., Advances in Agronomy, vol. 20, 1–50. Academic Press, Inc., New York.
———(1989) Phosphate reactions with natural allophane, ferrihydrite and goethite. Journal of Soil Science, 40, 359–369.
Peterson, M.L. and Carpenter, R. (1986) Arsenic distributions in porewaters and sediments of Puget Sound, Lake Washington, the Washington Coast and Saanich Inlet, B.C. Geochimica et Cosmochimica Acta, 50, 353–369.
Pichler, T. (1998) Shallow-water hydrothermal activity in a coral-reef ecosystem, Ambitle Island, Papua New Guinea. Ph.D. thesis, Department of Earth Sciences, Univerity of Ottawa, p. 206.
Pichler, T. and Dix, G.R. (1996) Hydrothermal venting within a coral reef ecosys-

tem, Ambitle Island, Papua New Guinea. Geology, 20, 435–438.
Pichler, T. and Veizer, J. (1999) Precipitation of Fe(III) oxyhydroxide deposits from shallow-water hydrothermal fluids in Tutum Bay, Ambitle Island, Papua New Guinea. Chemical Geology, 162, 15–32.
Pichler, T., Veizer, J., and Hall, G.E.M. (1999a) Natural input of arsenic into a coral-reef ecosystem by hydrothermal fluids and its removal by Fe(III) oxyhydroxides. Environmental Science and Technology, 33, 1373–1378.
———(1999b) The chemical composition of shallow-water hydrothermal fluids in Tutum Bay, Ambitle Island, Papua New Guinea and their effect on ambient seawater. Marine Chemistry, 64, 229–252.
Pierce, M.L. and Moore, C.B. (1982) Adsorption of arsenite and arsenate on amorphous iron hydroxide. Water Research, 16, 1247–1253.
Pollard, R.J., Cardile, C.M., Lewis, D.G., and Brown, L.J. (1992) Characterization of FeOOH polymorphs and ferrihydrite using low-temperature, applied-field, Mössbauer spectroscopy. Clay Minerals, 27, 57–71.
Quin, T.G., Long, G.L., Benson, C.G., Mann, S., and Williams, R.J.P. (1988) Influence of silicon and phosphorus on structural and magnetic properties of synthetic goethite and related oxides. Clays and Clay Minerals, 36, 165–175.
Rancourt, D.G. (1994) Mössbauer spectroscopy of minerals I. Inadequacy of Lorentzian-line doublets in fitting spectra arising from quadrupole splitting distributions. Physics and Chemistry of Minerals, 21, 244–249.
———(1998) Mössbauer spectroscopy in clay science. Hyperfine Interactions, 117, 3–38.
Rancourt, D.G. and Daniels, J.M. (1984) Influence of unequal magnetization direction probabilities on the Mössbauer spectra of superparamagnetic particles. Physical Review B, 29, 2410–2414.
Rancourt, D.G. and Ping, J.Y. (1991) Voigt-based methods for arbitrary-shape static hyperfine parameter distributions in Mössbauer spectroscopy. Nuclear Instruments and Methods in Physics Research B, 58, 85–97.
Rancourt, D.G., Julian, S.R., and Daniels, J.M. (1985) Mössbauer characterization of very small superparamagnetic particles: Application to intra-zeolitic α-Fe_2O_3 particles. Journal of Magnetism and Magnetic Materials, 49, 305–316.
Rancourt, D.G., Meschi, C., and Flandrois, S. (1986) S = 1/2 antiferromagnetic finite chains effectively isolated by frustration: $CuCl_2$–intercalated graphite. Physical Review B, 33, 347–355.
Rancourt, D.G., Dang, M.-Z., and Lalonde, A.E. (1992) Mössbauer spectroscopy of tetrahedral Fe^{3+} in trioctahedral micas. American Mineralogist, 77, 34–43.
Rancourt, D.G., Ping, J.Y. and Berman, R.G. (1994a) Mössbauer spectrocopy of minerals III. Octahedral-site Fe^{2+} quadrupole splitting distributions in the phlogopite-annite series. Physics and Chemistry of Minerals, 21, 258–267.
Rancourt, D.G., Christie, I.A.D., Royer, M., Kodama, H., Robert, J.-L., Lalonde, A.E. and Murad, E. (1994b) Determination of accurate $^{[4]}Fe^{3+}$, $^{[6]}Fe^{3+}$, and $^{[6]}Fe^{2+}$ site populations in synthetic annite by Mössbauer spectroscopy. American Mineralogist, 79, 51–62.
Randall, S.R., Sherman, D.M., Ragnarsdottir, K.V., and Collins, C.R. (1999) The mechanism of cadmium surface complexation on iron oxyhydroxide minerals. Geochimica et Cosmochimica Acta, 63, 2971–2987.
Raven, K.P., Jain, A., and Loeppert, R.H. (1998) Arsenite and arsenate adsorption on ferrihydrite: Kinetics, equilibrium, and adsorption envelopes. Environmental Science and Technology, 32, 244–349.
Rea, B.A., Davis, J.A., and Waychunas, G.A. (1994) Studies of the reactivity of the ferrihydrite surface by iron isotopic exchange and Mössbauer spectroscopy. Clays and Clay Minerals, 42, 23–34.
Rona, P.A. (1988) Hydrothermal mineralization at oceanic ridges. Canadian Mineralogist, 26, 431–465.
Saleh, A.M. and Jones, A.A. (1984) The crystallinity and surface characteristics of synthetic ferrihydrite and its relationship to kaolinite surfaces. Clay Minerals, 19, 745–755.
Saraswat, I.P., Vajpei, A.C., and Garg, V.K. (1977) Mossbauer resonance study of brown ferric oxyhydroxide gel. Indian Journal of Chemistry, Section a, 15, 493–494.
Scheinost, A.C., Chavernas, A., Barron, V., and Torrent, J. (1998) Use and limitations of second-derivative diffuse reflectance spectroscopy in the visible to near-infrared range to identify and quantify Fe oxide minerals in soils. Clays and Clay Minerals, 46, 528–536.
Schwertmann, U. and Murad, E. (1988) The nature of an iron oxide-organic iron association in a peaty environment. Clay Minerals, 23, 291–299.
St-Pierre, T.G., Bell, S.H., Dickson, D.P.E., Mann, S., Webb, J., Moore, G.R., and Williams, R.J.P. (1986) Mossbauer spectroscopic studies of the cores of human, limpet and bacterial ferritins. Biochimica Et Biophysica Acta, 870, 127–134.
St-Pierre, T.G., Webb, J., and Mann, S. (1989) Ferritin and hemosiderin: Structural and magnetic studies of the iron core. In S. Mann, J. Webb, and R.J.P. Williams, Eds., Biomineralization—chemical and biochemical perspectives, p. 295–344. VCH Publishers, Weinheim, Germany.
St-Pierre, T.G., Chan, P., Bauchspiess, K.R., Webb, J., Betteridge, S., Walton, S., and Dickson, D.P.E. (1996) Synthesis, structure and magnetic properties of ferritin cores with varying composition and degrees of structural order: models of iron oxide deposits in iron-overload diseases. Coordination Chemistry Reviews, 151, 125–143.
Thibault, P.-J. (2001) Biogenic and abiotic ferrihydrite. M.Sc. thesis, University of Ottawa, Ottawa, Canada (in French).
Van Cappellen, P. and Wang, Y. (1996) Cycling of iron and manganese in surface sediments: a general theory for the coupled transport and reaction of carbon, oxygen, nitrogen, sulfur, iron, and manganese. American Journal of Science, 296, 197-243.
Vandenberghe, R.E., De Grave, E., Landuydt, C., and Bowen, L.H. (1990) Some aspects concerning the characterizaton of iron oxides and hydroxides in soils and clays. Hyperfine Interactions, 53, 175–196.
Van Der Giessen, A.A. (1967) Magnetic properties of ultra-fine iron (III) oxide-hydrate particles prepared from iron (III) oxide-hydrate gels. Journal of the Physics and Chemistry of Solids, 28, 343–346.
Vempati, R.K., Loeppert, R.H., Sittertz-Bhatkar, H., and Burghardt, R.C. (1990) Infrared vibrations of hematite formed from aqueous- and dry-thermal incubation of Si-containing ferrihydrite. Clays and Clay Minerals, 38, 294–298.
Wallace, D.A., Johnson, R.W., Chappell, B.W., Arculus, R.J., Perfit, M.R., and Crick, I.H. (1983) Cainozoic volcanism of the Tabar, Lihir, Tanga, and Feni islands, Papua New Guinea. Geology, whole-rock analyses, and rock-forming mineral compositions, vol. 243, p. 62. Bureau of Mineral Resources Geology and Geophysics, Sydney.
Waychunas, G.A., Rea, B.A., Fuller, C.C., and Davis, J.A. (1993) Surface chemistry of ferrihydrite: Part 1. EXAFS studies of the geometry of coprecipitated and adsorbed arsenate. Geochimica and Cosmochimica Acta, 57, 2251–2269.
Waychunas, G.A., Davis, J.A., and Fuller, C.C. (1995) Geometry of sorbed arsenate on ferrihydrite and crystalline FeOOH: Re-evaluation of EXAFS results and topological factors in predicting sorbate geometry, and evidence for monodentate complexes. Geochimica and Cosmochimica Acta, 59, 3655–3661.
Waychunas, G.A., Fuller, C.C., Rea, B.A., and Davis, J.A. (1996) Wide angle X-ray scattering (WAXS) study of "two-line" ferrihydrite structure: Effect of arsenate sorption and counterion variation and comparison with EXAFS results. Geochimica and Cosmochimica Acta, 60, 1765–1781.
Weidner, V.R. and Hsia, J.J. (1981) Reflection properties of pressed polytetrafluoroethylene powder. Journal of the Optical Society of America, 71, 856–861.
Wilkie, J.A. and Hering, J.G. (1996) Adsorption of arsenic onto hydrous ferric oxide: Effects of adsorbate/adsorbent ratios and co-occurring solutes. Colloids and Surfaces A: Physicochemical and Engineering Aspects, 107, 97–110.
Winnik, F.M., Morneau, A., Mika, A.M., Childs, R.F., Roig, A., Molins, E., and Ziolo, R.F. (1998) Polyacrylic acid pore-filled microporous membranes and their use in membrane-mediated synthesis of nanocrystalline ferrihydrite. Canadian Journal of Chemistry, 76, 10–17.
Woolson, E.A. (1977) Fate of arsenicals in different environmental substrates. Environmental Health Perspectives, 19, 73–81.
Wyszecki, G. and Stiles, W.S. (1982) Color science: Concepts and methods, quantitative data and formulae, p. 950. Wiley, New York.
Ylagan, R.F., Altaner, S.P., and Pozzuoli, A. (2000) Reaction mechanisms of smectite illitization associated with hydrothermal alteration from Ponza Island, Italy. Clays and Clay Minerals, 48, 610–631.
Zhao, J., Huggins, F.E., Feng, Z., and Huffman, G.P. (1996) Surface-induced superparamagnetic relaxation in nanoscale ferrihydrite particles. Physical Review B, 54, 3403–3407.